

DNA nanotechnology: understanding and optimisation through simulation

Thomas E. Ouldridge¹

¹*Rudolf Peierls Centre for Theoretical Physics, University of Oxford Physics Department, 1 Keble Road, Oxford, OX1 3PG, UK, and Department of Mathematics, South Kensington Campus, Imperial College London, London, SW7 2AZ, UK.*

DNA nanotechnology promises to provide controllable self-assembly on the nanoscale, allowing for the design of static structures, dynamic machines and computational architectures. In this article I review the state-of-the art of DNA nanotechnology, highlighting the need for a more detailed understanding of the key processes, both in terms of theoretical modelling and experimental characterisation. I then consider coarse-grained models of DNA, mesoscale descriptions that have the potential to provide great insight into the operation of DNA nanotechnology if they are well designed. In particular, I discuss a number of nanotechnological systems that have been studied with oxDNA, a recently developed coarse-grained model, highlighting the subtle interplay of kinetic, thermodynamic and mechanical factors that can determine behaviour. Finally, new results highlighting the importance of mechanical tension in the operation of a two-footed walker are presented, demonstrating that recovery from an unintended ‘overstepped’ configuration can be accelerated by three to four orders of magnitude by application of a moderate tension to the walker’s track. More generally, the walker illustrates the possibility of biasing strand-displacement processes to affect the overall rate.

Key words: DNA nanotechnology; self-assembly; molecular machines; non-equilibrium systems; coarse-grained modelling; simulation.

*Correspondence: t.ouldridge@imperial.ac.uk

I. INTRODUCTION TO DNA NANOTECHNOLOGY

A. The DNA molecule and its potential

Deoxyribonucleic acid (DNA) is a macromolecule with a backbone of covalently linked sugar and phosphate groups; attached to each sugar is a base, which can be adenine (A), guanine (G), cytosine (C) or thymine (T)¹. DNA is often found as a double helix of antiparallel strands stabilised by hydrogen-bonding of complementary Watson-Crick base pairs (AT and CG) and stacking interactions between the planar bases. Double-stranded DNA (dsDNA) is stiff, with a persistence length of ~ 150 base pairs², whereas unpaired single strands (ssDNA) are far more flexible^{3,4}.

DNA carries information through its sequence of bases - in biology, this information codes for proteins and their regulation. The specificity of Watson-Crick base-pairing means that both strands within a duplex carry identical information, facilitating replication. In 1982, Seeman speculated that the specificity of DNA hybridization could be harnessed to permit the design of artificial structures, proposing that certain sequences could self-assemble into crystals⁵.

B. DNA nanostructures

The Seeman group quickly constructed artificial nucleic acid junctions⁶, but the first 3-dimensional crystal based purely on rationally designed Watson-Crick base pairs was not demonstrated until 2009⁷ (crystals involving non-canonical interactions were created in 2004⁸). In the intervening period, ribbons⁹ and 2D lattices^{10,11} were

realised. Complex Archimedean tiling patterns¹² and ‘empty liquids’¹³ have recently been achieved through hybridization-driven DNA self-assembly.

As well as macroscopic phases, DNA can form structures of well-defined finite size. Early successes (cubes¹⁴ and octahedra¹⁵) involved several discrete stages of assembly, but it was subsequently shown that polyhedra^{16,17,18} and then more complex structures^{19,20} could be made to form simply by cooling solutions of short ssDNA strands (oligonucleotides). An alternative approach, known as DNA ‘origami’²¹, uses one long ‘scaffold’ strand that is shaped by shorter ‘staple’ strands into a complex structure. This technique can produce three dimensional objects^{22,23} and structures with curvature or twist^{24,25}. Some examples of DNA nanostructures are shown in Fig. 1 (a)-(c).

DNA does not have to be used in isolation – it can also be conjugated with other molecules or nanoparticles. Crystals of DNA-coated colloids have been constructed²⁶, and small organic molecules have been used as vertices in structures held together by DNA^{27,28}.

C. Dynamic DNA devices

DNA is not restricted to static nanostructures, but can be used to create dynamically active nanoscale objects. Toehold-mediated strand displacement (TMSD), illustrated in Fig. 1(d), is used along with hybridisation to drive conformational changes in many such devices. TMSD involves the replacement of a strand (the *incumbent*) from a duplex with the *substrate* by an alternative strand (the *invader*) that is complementary to an additional *toehold* of the substrate. Initially, the

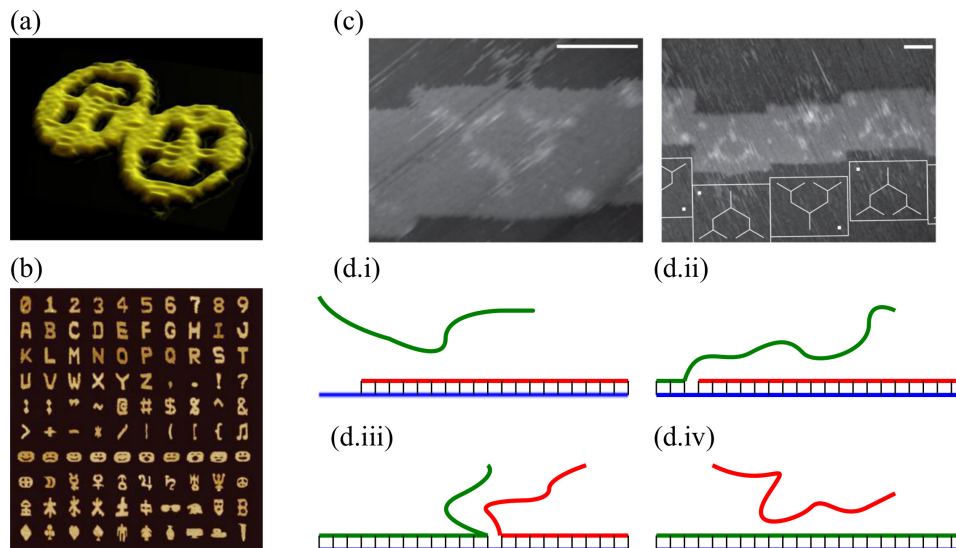


FIG. 1. (a)-(c) Examples of DNA nanotechnology. (a) Atomic force microscopy (AFM) image of the original DNA ‘origami’²¹, courtesy of P. W. K. Rothemund. (b) AFM of complex structures assembled from DNA ‘bricks’¹⁹, courtesy of P. Yin. (c) Tracks for a DNA-based motor on origami. Reprinted by permission from Macmillan Publishers Ltd: Nature Nanotechnology²⁹, copyright 2012. (d) Basic displacement. (d.i) The initial state with incumbent (red) and substrate (blue) bound, and the invader (green) free in solution. (d.ii) The invader binds to the available toehold of the substrate. (d.iii) The invader competes with the incumbent for base pairs. (d.iv) The final state, in which the invader has completely displaced the incumbent.

invader can bind to the exposed toehold, as shown in Fig. 1 (d.ii)^{30,31,32}. The invader and incumbent can then compete for base-pairing, as illustrated in Fig. 1 (d.iii). If, eventually, the incumbent loses all of its base pairs, it will detach and displacement is complete (Fig. 1 (d.iv)). As well as being essential in dynamic nanotechnology, displacement may occur during the assembly of complex structures that initially form unintended bonds between the wrong strands.

The simplest devices are switches that respond to a change in experimental conditions. An iconic example are the ‘tweezers’ of Yurke *et al.*³³, which can be closed and opened by sequential addition of ‘fuel’ strands (which bind to and closes the tweezers) and ‘antifuel’ strands (which displace the tweezers from the fuel, opening them). Switches can allow large structures to open, close or undergo topological rearrangement^{23,34,35,36}.

DNA ‘walkers’ couple the mechanical change generated by DNA reactions to motion along extended tracks, analogous to biological motors such as kinesin and myosin. The earliest designs used sequential strand addition to generate unidirectional motion along a series of binding sites (‘stators’)^{37,38}. Solution conditions can also be modulated in different ways, for example through periodic exposure to light of different frequencies³⁹. Autonomous motors, which don’t rely on external control, must catalyse the release of free energy⁴⁰. To meet this requirement, designs often couple motion to the hydrolysis of a nucleic acid strand that is not part of the walker itself. Hydrolysis can be achieved either with^{41,42,43} or without^{44,45,46} the involvement of an additional enzyme. An alternative is to catalyse DNA hybridisation itself^{47,48} if the re-

actants are present as metastable self-bonded hairpins. Many walkers destroy the track behind them in the so-called ‘burnt bridges’ approach. The Turberfield group have also demonstrated the possibility of autonomous motion on a track that can be reused^{42,47}. In the majority of cases, hybridisation and displacement are central to walker operation, sometimes in combination with additional enzymatic reactions. An alternative is to use four-way branch migration rather than displacement^{49,50}.

A third branch of active DNA nanotechnology is computation. In 1994 Adleman showed that a Hamiltonian path problem could be solved using DNA⁵¹. Subsequently, researchers have developed motifs for logical operation based on TMSD⁵², with the Winfree group having incorporated multiple gates into a decision-making ‘brain’⁵³, and Chen *et al.* having developed a general architecture for control networks⁵⁴.

D. Applications of DNA nanotechnology

Many nanotechnological systems are elegant proofs of principle, rather than being directly useful. The potential of DNA nanotechnology, however, is obvious. Seeman’s original motivation was to use DNA crystals to conjugate proteins and facilitate crystallography; origami bundles and two-dimensional lattices have indeed been used to aid protein structure determination^{55,56}. Similarly, finite-sized nanostructures contain unique strands at well-defined locations. This allows nanostructures to function as nanoscale breadboards for biophysical systems – they have been used as backbones for plas-

monic devices⁵⁷ and light-harvesting complexes⁵⁸, to control^{59,60} and facilitate the study of^{61,62,63} enzymatic reactions, and to provide tracks for DNA motors^{29,64} (as shown in Fig. 1 (c)). DNA nanostructures have also been designed to act as microscopic gene-detecting arrays^{65,66}. The freedom to design complex structures allows DNA to be used for other experimental components, including ‘handles’, ‘frames’ and ‘rulers’ for single-molecule manipulation^{67,68}, and harnesses for arrays of motor proteins⁶⁹.

The therapeutic potential of DNA nanotechnology has long been recognised. Nanostructures can encapsulate molecules either covalently or non-covalently^{70,71}, with the aim of selectively releasing them at the surface of or inside specific cells. Alternatively, nanostructures can coordinate biomolecules to mimic pathogens, potentially triggering stronger immune responses^{72,73,74} and allowing the design of novel vaccines⁷². DNA computation may also prove to be most valuable in medical applications, when its enormous parallel capacity and direct interaction with biomolecules will prove most advantageous. Towards this end, both the uptake of small nanostructures into cells^{73,75,76} and specific targeting of cancer cells by DNA-transported drugs⁷⁰ have been demonstrated. Large DNA nanostructures have been reported to be survive intact in cell lysate⁷⁷, and DNA-based devices and structures have been shown to be stable within *C. elegans* for hours or days, depending on the design⁷⁸. The Shih lab has also shown that lipid encapsulation of nanostructures can help to shield them from digestion by nucleases when this is an issue⁷⁹ and coating origami with virus capsid proteins has been shown to improve transfection into cells⁸⁰. Interacting “robots” have even been demonstrated to perform computations based on TMSD within a living organism⁸¹.

Artificial walking devices could function as agents in molecular assembly lines, incorporating some degree of decision-making. Preliminary work has demonstrated that DNA hybridisation can accelerate and template reactions^{82,83}, that walkers can make decisions at junctions^{29,50} and that walkers can selectively pick up gold nanoparticle cargo⁸⁴.

E. Understanding and optimising DNA nanotechnology

If DNA nanotechnology is to be widely used, assembly processes and operation cycles must be understood and optimised. Simple self-assembling structures such as DNA tetrahedra form reliably when a solution of reactants is rapidly cooled¹⁶. Larger systems tend to be more complex, although recent work has shown that substantial structures can form surprisingly well if the temperature is carefully chosen^{85,86}. It is not obvious, however, why assembly can be so successful given previous failures with large colloidal structures⁸⁷. It is also not clear why origami assembly can occur over a very narrow temperature window⁸⁵, with significant hysteresis^{85,88}. Im-

proving yields of larger structures by choosing sequences to minimise unintended cross-interactions has shown surprisingly little promise thus far^{19,20}, but origami assembly is very sensitive to the staple layout^{86,89,90}. Even if an object appears to form well, some strands might be absent, possibly compromising its usefulness and mechanical properties⁹¹. Optimisation is even more important for dynamic nanotechnology, where relatively slow unintended reactions can compromise device operation⁶⁴. For example, even if a walker has only a 5% chance of detaching from the track at each step, most will fail to take twenty steps. As it stands, motors are slow compared to natural analogs, and systematic approaches for improving their effectiveness or decision-making abilities are currently limited.

Recent experiments have probed specific systems relevant to nanotechnology in detail^{31,64,85,86,89,90,92,93,94}. To interpret these results, generalise the resultant ideas and develop new principles, these systems must be modelled theoretically. To date, the main theoretical tool has been the nearest-neighbour model of DNA thermodynamics⁹⁵, implemented in online tools such as NuPack⁹⁶. The nearest-neighbour model functions at the level of secondary structure (*i.e.*, lists of the base-pairing that is present in the system). The free energy of a given secondary structure can be estimated by summing contributions from each neighbouring ‘stack’ of base pairs, plus contributions from end effects and enclosed loops. Whilst the nearest-neighbour model is extremely useful, it has several limitations. Firstly, it is a thermodynamic model with discrete states and hence has no natural kinetics³². Secondly, it does not explicitly represent DNA structure, and struggles to describe complex interconnections, loops and ‘pseudoknots’⁹⁶ that often arise in nanotechnological systems. Finally, DNA mechanics is ignored, meaning that the effects of forces and torques cannot be directly understood.

Next, I will introduce coarse-grained models of DNA, mesoscale representations that can overcome the limitations of the nearest-neighbor description. I will focus on oxDNA, a model explicitly designed for DNA nanotechnology. I will outline the model, before discussing previous applications in understanding TMSD in a variety of contexts. Finally, new results will be presented on displacement involving a two-footed DNA walker⁴², highlighting the possibility of accelerating displacement through mechanical strain.

II. COARSE-GRAINED MODELLING OF DNA NANOTECHNOLOGY

Coarse-grained models provide a level of resolution between fully atomistic treatments and secondary-structure descriptions like the nearest-neighbour model. Atomistic treatments are generally too computationally expensive for nanotechnological applications, although some structural studies have been performed^{97,98}. Coarse-grained

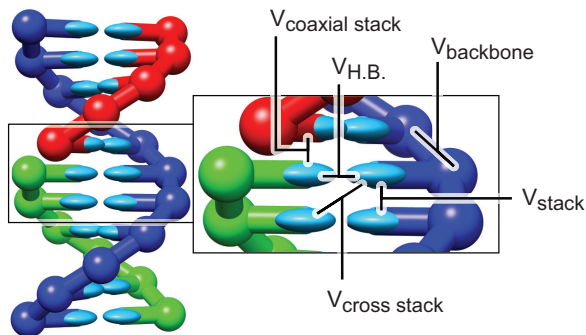


FIG. 2. Illustration of the duplex structure and stabilising interactions with the oxDNA model. Spheres represent the backbone sites, and ellipsoids represent bases. Strands are coloured according to their identity. Coaxial stacking acts like a nearest-neighbour stacking interaction between bases that are not consecutive on the same strand. Excluded volume interactions (not illustrated here) also exist between all backbone and base sites. Reprinted with permission from T.E. Ouldridge, *et al.*, Optimizing DNA nanotechnology through coarse-grained modelling: A two-footed DNA walker, ACS Nano 7, 2479. Copyright (2013) American Chemical Society.

models represent individual nucleotides using a small number of interaction sites, which interact through effective potentials. If well parameterised, they can capture the known thermodynamic, structural and mechanical properties of DNA in a simple and naturally dynamical representation.

The choice of interactions determines the accuracy and applicability of the model. A ‘bottom-up’ approach is to fit interactions to reproduce correlation functions from more detailed atomistic simulations^{99,100,101,102,103,104,105,106,107,108,109,110,111,112,113}, or data from experimentally determined structures^{99,108,114,115}. This procedure can be very effective, but it has limitations. Firstly, the resultant model is very dependent on the source data, which are usually primarily drawn from duplex DNA, whereas nanotechnological systems involve ssDNA and hybridisation transitions (one exception has focused specifically on ssDNA only¹¹¹). Even if a wider variety of systems were to be used for parameterisation, it is not clear whether current atomistic representations accurately describe isolated ssDNA and the hybridisation transition. Secondly, one cannot retain all features of a system when coarse-graining; ‘representability problems’ arise¹¹⁶. For a given set of coarse-grained degrees of freedom, the optimal potential for correlation functions will likely be distinct from that for thermodynamics. Related issues are relevant to potentials derived from *ab initio* calculations¹¹⁷.

Representability problems highlight the fact that coarse-grained models cannot be perfect, and hence should be designed with their purpose in mind. For nanotechnological systems, models must capture ss-

DNA, dsDNA and their interconversion. To date, this has been most successfully done with ‘top-down’ approaches^{118,119,120,121,122,123,124,125,126,127,128,129,130,131,132,133,134,135}. Here, physically-motivated interactions such as hydrogen-bonding and stacking are included and parameterised to reproduce overall thermodynamic, mechanical and structural properties of DNA. In this article I focus on oxDNA^{137,138,139}, an attempt to incorporate thermodynamics as parameterised by the nearest-neighbour model into a description with continuous degrees of freedom that captures structural and mechanical properties of DNA. Due to the emphasis placed on capturing the duplex formation transition in the development of oxDNA, it has been used to study nanotechnological systems more extensively than other models. However, duplex and hairpin formation transitions have been systematically investigated by a number of groups^{119,120,121,123,124,127,130,132,140,141,142,143,144}, nanostructure conformation has been studied by Bombelli *et al.* and Arbona *et al.*^{136,145}, and nanostructure assembly^{146,147,148} and displacement¹⁴⁹ have been demonstrated with much simple models of DNA. Large-scale assembly of DNA-coated objects has also been achieved with some simpler coarse-grained models^{120,135,150}. It is worth noting that similar top-down^{132,151,152,153,154,155,156,157} and bottom-up^{158,159,160,161} models exist for RNA.

1. oxDNA

oxDNA treats each nucleotide as a 3-dimensional rigid body. The potential energy of a configuration is given by

$$V = \sum_{\langle ij \rangle} (V_{b.b.} + V_{stack} + V'_{exc}) + \sum_{i,j \notin \langle ij \rangle} (V_{HB} + V_{cr.st.} + V_{exc} + V_{cx.st.}). \quad (1)$$

Here the first sum runs over all consecutive pairs of nucleotides on a strand, and the second sum over all remaining pairs. The interactions represent hydrogen bonding (V_{HB}), cross stacking ($V_{cr.st.}$), coaxial stacking ($V_{cx.st.}$), nearest-neighbour stacking (V_{stack}), excluded volume (V_{exc} or V'_{exc}) and backbone chain connectivity ($V_{b.b.}$). These interactions are shown schematically in Fig. 2, and are discussed in detail elsewhere^{137,138,139}. Importantly, attractive interactions depend explicitly on the relative orientations of nucleotides, allowing the anisotropic nature of bases to play a role.

Hydrogen-bonding and stacking interactions drive the formation of duplexes with helical structure from single strands that are relatively more disordered. oxDNA reproduces the thermodynamic, mechanical and structural changes associated with this transition, under high salt conditions. In particular, oxDNA provides a good representation of duplex melting temperatures, melting transitions widths, self-complementary hairpin

stability, duplex elastic moduli and the short persistence length of single strands (details are provided in Refs.^{137,138,139}). Our group uses the “Virtual Move Monte Carlo” (VMMC) algorithm (the variant in the appendix of Ref.¹⁶²) to calculate model thermodynamics. Dynamical properties require an additional choice of model kinetics; we use Langevin¹⁶³ and Andersen-like¹⁶⁴ thermostats. To improve sampling, our group has made extensive use of umbrella sampling (US)¹⁶⁵ for thermodynamic averages and forward flux sampling (FFS)^{166,167} for kinetic studies.

Several important simplifications are inherent in the model. Firstly, oxDNA was fitted at a salt concentration of $[\text{Na}^+] = 0.5\text{ M}$ where electrostatics is strongly screened – the repulsion of phosphates is therefore incorporated into the backbone excluded volume for simplicity. A recent study by the Pettitt group¹⁶⁸ has explored the possibility of incorporating a Debye-Hückel description of electrostatics, allowing lower salt conditions to be simulated, but the results reported in this work do not include this term. Secondly, model duplexes are symmetric, meaning that both grooves of the helix are the same size. Such a simplification may be of relevance when systems are extremely sensitive to geometric details; for example, the stress imposed on helices by crossovers at origami junctions will be affected by grooving. Thirdly, as nanotechnology typically involves low concentrations of DNA, oxDNA takes the partial pressure of strands to be zero. Therefore simulations of DNA with implicit solvent in the canonical ensemble are appropriate for comparisons to typical experimental systems at constant temperature and pressure¹⁶⁹. Consistent with this picture, we interpret free energies measured in simulations as Gibbs (rather than Helmholtz) free energies. Finally, the Langevin and Andersen-like thermostats do not incorporate collective hydrodynamic motion, and low friction coefficients are typically used to accelerate dynamics. Given these and other simplifications, it is important to identify the underlying cause of any phenomena observed in simulation, to ensure that they arise from real DNA physics rather than artefacts of the model or dynamical algorithm.

III. INSIGHTS INTO STRAND DISPLACEMENT FROM OXDNA

I now outline how oxDNA has been used to understand basic TMSD, and then to explore variants relevant to nanotechnology.

A. Basic displacement

TMSD was experimentally characterised by Zhang and Winfree³¹. These authors demonstrated that for short toeholds, displacement rate increases exponentially with toehold length, before plateauing in the long toehold

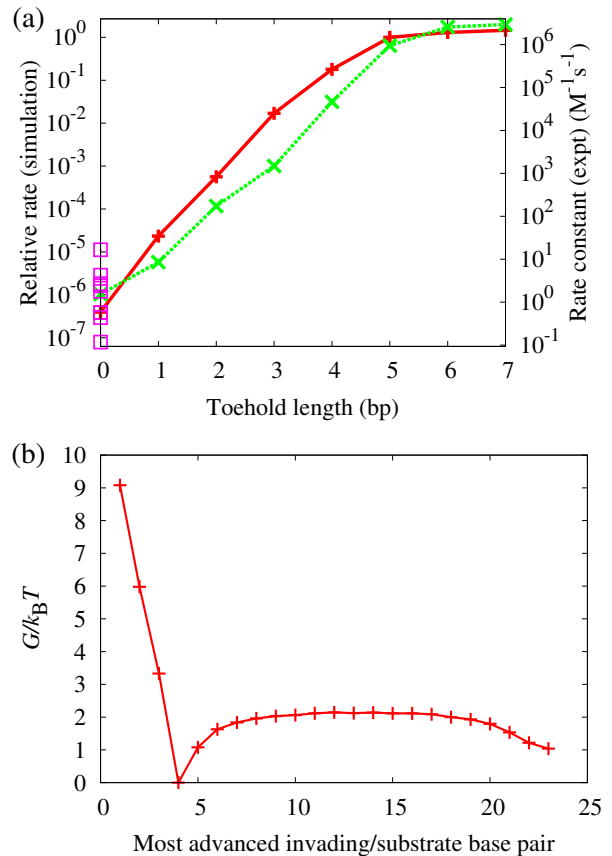


FIG. 3. (a) Experimentally measured rate constants as a function of length for an average-strength toehold³¹ (green ‘x’ symbols), compared to the relative displacement rates found for oxDNA (red ‘+’ symbols, reported relative to the 5 base-pair case)³². Purple squares show the new estimates of zero-toehold displacement rate for oxDNA presented in this work (detailed in the Supplementary Material), showing substantial measurement uncertainty. Although not quantified here, this uncertainty is much smaller for longer toeholds, when the process is easier to sample³². The minor variation between rates for long toeholds demonstrates the small error in this limit. (b) Free energy (G) profile of displacement in oxDNA as a function of the most advanced invader/substrate base pair for a four-base toehold. Base pair ‘1’ is at the far end of the toehold from the displacement domain, and base pair 4 is immediately adjacent to the displacement domain³². Typical errors on these measurements are smaller than the ‘+’ symbols, as estimated through comparison of independent simulations³².

limit. The results, a subset of which are reproduced in Fig. 3 (a), show that displacement accelerates by a factor of $\sim 10^{6.5}$ as the toehold is increased from 0 to 15 base pairs (for a displacement domain of 20 base pairs, at 25°C and with a high salt concentration of $[\text{Mg}^{2+}] \approx 10\text{ mM}$). The overall shape of the graph is unsurprising. At the low strand concentrations used in Ref.³¹, the three-stranded intermediate (including states depicted in Figs. 4 (a.ii), (a.iv) and (b)) is short-lived and the reaction is effectively second order. In this limit, the reaction rate constant can be modelled as

$$k_{\text{eff}} = k_{\text{bind}} P_{\text{suc}}, \quad (2)$$

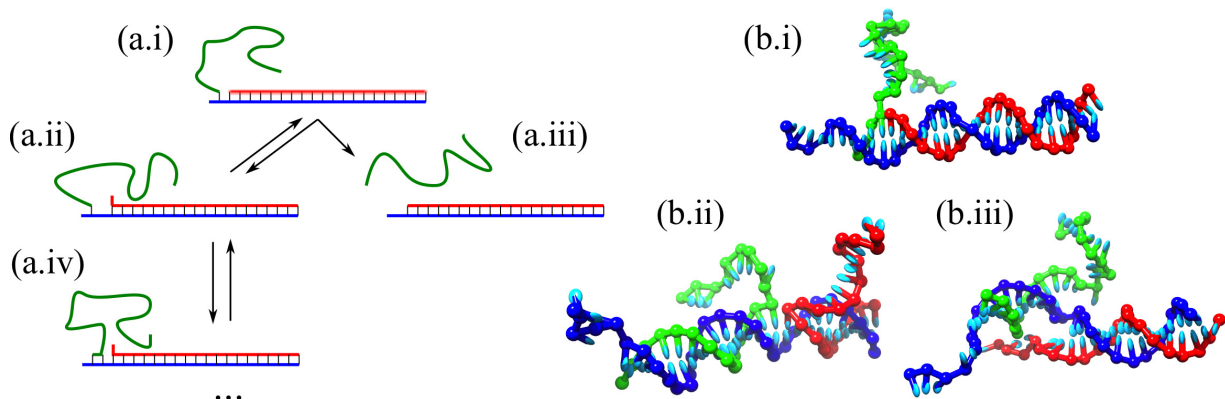


FIG. 4. Representations of displacement at two levels of detail. In both cases the substrate is blue, the invader green and the incumbent red. (a) Illustration of a simple step-by-step model of displacement for a one-base toehold. Starting from the toehold-bound state (a.i), either a base pair between incumbent and substrate can break (a.ii) or the toehold base pair can break, leading to detachment (a.iii). From state (a.ii), either the invader can bind to the newly revealed substrate base (a.iii), or the incumbent can rebind, returning us to the initial state (a.i). This process can be repeated for every base in the displacement domain. (b) Displacement in oxDNA (for a three-base toehold). (b.i) The toehold-bound state. (b.ii) A later stage of displacement. (b.iii) A later stage of displacement in which the invader and incumbent duplexes have unstacked at the displacement junction.

where k_{bind} is a toehold binding rate constant and P_{suc} is the probability that displacement succeeds (as opposed to the invader detaching) once the toehold is formed. For very short toeholds it is reasonable that $P_{\text{suc}} \ll 1$. Increasing the toehold length increases the toehold stability, and hence P_{suc} , exponentially. Eventually this increase with toehold length saturates when $P_{\text{suc}} \sim 1$. Given that k_{bind} would be expected to be relatively weakly length-dependent, k_{eff} therefore plateaus at this point.

A simple argument, however, would suggest that a single-base toehold should have a success rate greater than 1%, thereby limiting the possibilities for increasing k_{eff} by increasing the toehold length and hence P_{suc} . Consider the system illustrated in Fig. 4 (a), with a toehold of one base, and assume that displacement is a random walk in which base pairs at the junction can break and then be replaced by base pairs with the competing strand, as shown in Fig. 4(a). From the toehold-bound state, two things can happen – either the toehold detaches, or the first base pair in the incumbent/substrate breaks. If the latter, the invader then takes a base pair from the incumbent 50% of the time, otherwise the system returns to the initial state. If toehold detachment (involving the disruption of a single base pair), and breaking of base pairs at the junction have similar rates, the probability that the invader manages to take the first step is then approximately 1/3. From here, 19 more displacement steps are required, whereas the initial state is one backwards step away. From the statistics of random walks, we obtain $P_{\text{suc}} \sim \frac{1}{3} \frac{1}{20} \sim 0.02$ for single-base toeholds. Given this estimated value of P_{suc} for a single-base toehold, it is difficult to justify the extent of the experimentally observed slowdown for shorter toeholds.

The displacement process has been simulated with oxDNA, as outlined in Ref.³². The results shown in

Fig. 3(a) agree well with those obtained by Zhang and Winfree. The key point, however, is not the quality of agreement, but that oxDNA also violates the simple argument outlined above which suggests only a modest slowdown for short toeholds. By studying oxDNA, we can then hope to explain the experimental results. Explanations for this behaviour, violations of two assumptions of our simple argument, are given discussed in detail Ref.³².

Firstly, junction migration is not an unbiased random walk. As junction migration is initiated, a second single-stranded section is generated at the displacement junction, as can be seen in Fig. 4(b). This second overhang is thermodynamically unfavourable, due to steric exclusions at the junction, and consequently biases the system against initiating and proceeding with junction migration. It therefore reduces the probability of successful displacement given toehold binding. A free-energy profile indicating a thermodynamic cost for initiating displacement is shown in Fig. 3(b) (the free energy as a function of an order parameter, $G(Q)$, is a measure of the probability that the system exists in state Q , $P(Q)$: $G(Q) = -k_{\text{B}}T \ln P(Q) + \text{const}$).

Secondly, simulations show that junction migration is far more complex than the breaking of a single base pair in the toehold, necessarily involving the disruption of more stacking interactions and a greater structural rearrangement. Junction migration is then intrinsically slow compared to the disruption of toehold base pairs, again reducing the probability of displacement as opposed to detaching from the toehold.

The Winfree group have used the thermodynamic stability of ‘frozen’ displacement intermediates to explore the possibility of the penalty associated with dangling ssDNA at the junction, confirming its existence and estimating a value of $\sim 3k_{\text{B}}T$, slightly larger than found for oxDNA³². Analysis of a simple secondary-structure

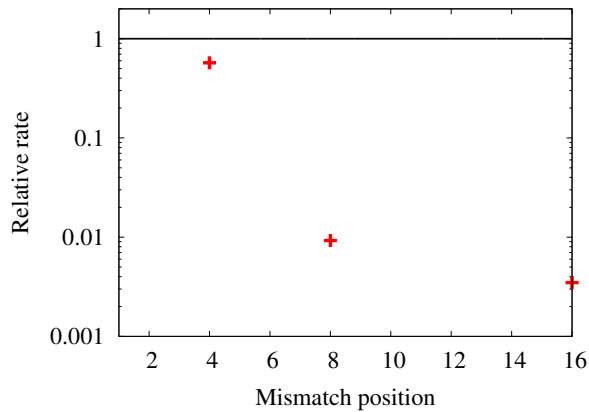


FIG. 5. Relative rates of displacement as a function of the position of a mismatch created during displacement (as predicted by oxDNA)¹⁷⁰. The position is defined with respect to the far end of the displacement domain (which has a length of 16 base pairs in this system) – a mismatch at position ‘16’ is immediately adjacent to the toehold, and a mismatch at position ‘4’ is near the far end of the displacement domain. Values are reported relative to the rate for a perfectly matched invader, and the all points are estimated to have an error less than or equal to a factor of 2, as estimated through independent simulations¹⁷⁰.

based model³² suggests that such an impediment provides only a partial explanation of the degree to which longer toeholds can accelerate displacement. As a consequence, the second factor identified by oxDNA as inhibiting displacement (slow junction migration) seems necessary to explain the wide range of rates as a function of toehold length.

B. Displacement involving mismatches

The plateau in displacement rate as toehold length increases limits the maximal selectivity for intended processes over leak reactions. Modifying displacement to reduce its success probability would enlarge the regime in which rate grows with toehold stability, and hence the dynamic range and maximal selectivity. Authors have included physical separation of the toehold from the displacement domain¹⁷¹ or forced the invading strand to create unfavourable ‘mismatched’ base pairs^{172,173} to achieve this. The principle is generally to slow displacement by decreasing the overall free-energy gain $|\Delta G^{\text{disp}}|$ of the reaction.

OxDNA has been used to simulate displacement in which a C-G base pair is replaced by a C-C mismatch as displacement proceeds¹⁷⁰. Mismatches were considered at the start, in the middle, and four base pairs from the end of a 16-base displacement domain, for a toehold of 5 bases. In each case, the mismatch destabilises the final invader/substrate duplex by approximately $\Delta\Delta G_{\text{mm}}^{\text{disp}} = 5.9k_{\text{B}}T$. We might then naively expect

a rate reduction by a factor

$$\frac{k_{\text{eff}}^{\text{mm}}}{k_{\text{eff}}^{\text{perfect}}} \approx \exp(-\Delta\Delta G_{\text{mm}}^{\text{disp}}/k_{\text{B}}T) \approx \frac{1}{350} \quad (3)$$

The results, taken from Ref.¹⁷⁰ and shown in Fig. 5, are initially surprising. The early mismatch does indeed cause a slowdown by ~ 350 , and the middle mismatch by a factor ~ 100 . The late mismatch, however, has almost no influence. This result must mean that P_{suc} is high despite the late mismatch. The fact that the mismatch is far from the toehold certainly helps – after encountering the mismatch, the junction must migrate 12 steps backwards before the invader is bound only to the toehold, raising the probability that displacement will occur anyway despite the impediment. However, mismatches are so destabilising ($5.9k_{\text{B}}T$ in this case) that it is still difficult to see how enclosing it and subsequently completing junction migration would not be slow compared to returning to the toehold-only state. The resolution of this paradox is the existence of an alternative pathway, in which the incumbent strand spontaneously detaches from the substrate at a stage when the invader has not yet enclosed the mismatch. This pathway should be contrasted with the standard picture of base-by-base displacement³². The invader/substrate base pairs beyond the mismatch are then formed at a later stage, when there is no competition from the incumbent, and the full penalty of $\Delta\Delta G_{\text{mm}}^{\text{disp}}$ is not manifest in the displacement reaction rate. This alternative pathway is illustrated schematically, and contrasted with a displacement pathway which involves enclosing the mismatch, in Fig. 6.

Spontaneous detachment involves breaking a number of base pairs. When the mismatch is late in the displacement domain, it is feasible for the incumbent to detach spontaneously when the invader reaches the mismatch location. This process is somewhat analogous to the detachment of a short toehold, as discussed in Section III A. As highlighted in Section III A, toehold detachment is relatively fast compared to completing displacement; this explains why spontaneous detachment involving the disruption of several base pairs can be a kinetically favoured pathway, even when the most stable final state involves enclosure of the mismatch by the invader/substrate duplex.

As the mismatch is moved towards the start of the displacement domain, the number of base pairs that must break spontaneously grows and the rate of detaching in this way is exponentially suppressed. Eventually, spontaneous detachment is so slow that it is no longer faster than simply continuing displacement in the conventional base-by-base manner, and enclosing the mismatch. For oxDNA, both the middle and early mismatches are in this regime and hence they feel the effect of $\Delta\Delta G_{\text{mm}}^{\text{disp}}$. The difference between middle and early mismatches arises not from differences in the rate at which displacement occurs given toehold binding, but actually due to slower toehold detachment for the middle mismatch¹⁷⁰.

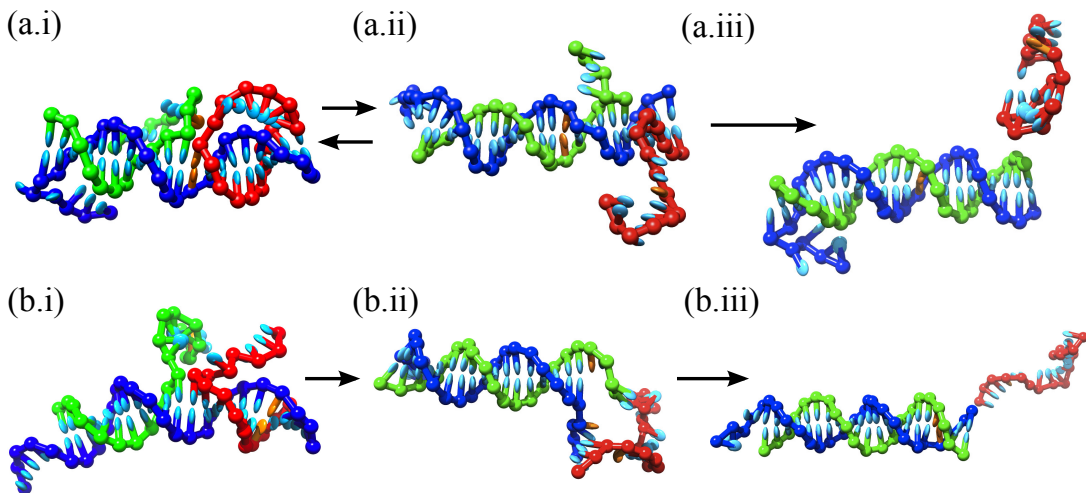


FIG. 6. Distinct pathways for displacement involving the creation of a mismatched base pair. The incumbent is shown in red, the invader in green and the substrate in blue. The location of the mismatch is highlighted by the orange-coloured bases. (a) Creating a mismatch in the middle of the displacement domain. The typical pathway involves enclosure of the mismatch (a.ii) prior to detachment of the incumbent and the completion of displacement (a.iii). (b) Creating a mismatch four bases from the end of the displacement domain typically involves detachment of the incumbent (b.ii) prior to enclosure of the mismatch (b.iii).

In general, oxDNA predicts that mismatches formed at the start of a displacement domain will heavily suppress displacement rates. Rates should initially rise slightly as the mismatch is moved towards the far end of the domain (away from the toehold). At some point, the spontaneous melting pathway will become relevant and the overall rate will rise rapidly, eventually plateauing at the perfectly-matched value. Recent experiments have demonstrated exactly this behaviour¹⁷⁰, showing that oxDNA is a powerful tool for probing DNA reaction dynamics.

These results emphasise that mismatches should be placed at the start of the displacement domain to slow displacement and thus suppress the rate of leak reactions. Recent work has considered using displacement to resolve single-nucleotide polymorphisms in genes^{66,174,175,176}; oxDNA suggests that the simplest kinetic methods might struggle to detect mutations at the end of a displacement domain^{66,174}, although modified approaches might fair better^{175,176}. More generally, the results illustrate a mechanism for modulating reaction kinetics by orders of magnitude whilst maintaining approximately the same overall reaction thermodynamics. A corollary is that reverse reactions will be far faster for the late mismatch, which may also be important when designing nanotechnological systems.

C. Displacement during the cycle of a burnt-bridges motor

OxDNA has been used¹⁷⁷ to model a burnt-bridges DNA motor designed by Turberfield and coworkers^{29,41,43}. The motor is illustrated in Fig. 7 (a). I will focus on the mechanism by which the motor strand (or ‘cargo’) steps from one stator (a single-stranded binding site anchored to the track) to the next via displace-

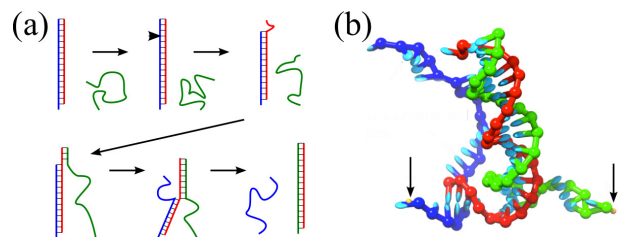


FIG. 7. The burnt-bridges motor introduced in Ref.⁴¹. (a) A schematic of motor operation. The cargo (red) is initially bound to the first stator (blue). A nicking enzyme cuts this stator, revealing a toehold (six bases in this case) for an alternative stator (green) which can displace the original, resulting in a step of the cargo strand. (b) An intermediate stage of stepping as represented by oxDNA. The two stators are anchored at points indicated by the vertical arrows. From this figure it is clear that the final stages of displacement involve subjecting the motor to considerable tension as it stretches between the two anchoring points.

ment - a simulation snapshot of this process is shown in Fig. 7 (b). The free-energy profiles of displacement, for various distances d_s between the stators, are shown in Fig. 8. As d_s is increased, toehold formation becomes slightly less favourable, due to a greater loss of entropy associated with toehold binding when the stators are further apart. Far more significant, however, is the rise in free energy at later stages that can be seen for large d_s . As displacement progresses, fewer bases are available to stretch across the gap between the points at which the stators are anchored, as shown in Fig. 7 (b). Displacement must then work against the tension of these stretched bases, meaning that the free energy rises as displacement progresses.

Some caution must be exercised when using free-energy profiles to infer kinetics. If the low-dimensional order pa-

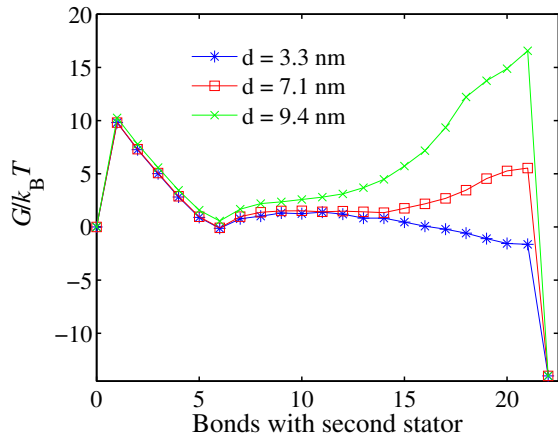


FIG. 8. Free-energy (G) profiles as a function of the number of bonds with the second stator during the displacement stage of the cycle of a burnt-bridges motor. Profiles are shown for three different separations between the anchoring points of the stators. Reprinted with permission from P. Šulc *et al.*, Simulating a burnt-bridges DNA motor with a coarse-grained DNA model, Natural Computing 1-13. Copyright (2013) Springer Science and Business Media¹⁷⁷.

parameter used is not a perfect reaction coordinate, signatures of kinetic effects may be hidden. Indeed, the relative difficulty of junction migration highlighted in Section III A is not easily identified in free-energy profiles at the level of base pairs. Nonetheless, large stator separation will clearly frustrate motor stepping, primarily due to lower rates of displacement once the toehold is formed, rather than slow toehold formation. Moderately large stator separations could then be used like early mismatches to reduce displacement success probabilities, thereby increasing the toehold length required to saturate P_{suc} at unity and suppressing leak reactions relative to the rate in this long-toehold limit. This approach would be particularly useful at junctions where decisions must be made²⁹. If d_s primarily influenced binding rates, rather than success probabilities, larger d_s would not help to discriminate between toeholds but would slow all reactions equally.

It is worth noting that slowing displacement by increasing d_s alters reaction kinetics without changing the overall ΔG of reaction. This is similar to changing the location of a mismatch formed between invader and substrate, but unlike increasing the number of mismatches. This is because the initial and final states, in which the cargo is bound to one stator only, are not d_s -dependent. Large values of d_s can in principle be used at an arbitrarily large number of stages for the same cargo molecule without destabilising the final product. This advantage of modulating kinetics with d_s must be weighed against the fact that the motif is limited to sequential reactions on a surface.

IV. RECOVERY OF A TWO-FOOTED WALKER: AN EXAMPLE OF ENHANCED DISPLACEMENT

The Turberfield group has also introduced a two-footed DNA walker that is designed to achieve directional motion without modifying its track, a continuous single strand consisting of multiple binding sites⁴². The walker is intended to step in a foot-over-foot fashion; its full design is given in Ref.⁴². It is intended to exist either with a single foot bound to the track and the other raised, or with both feet bound to overlapping adjacent sites, as illustrated in Fig. 9 (a) and (b). The feet must overlap, as competition means that one or other of the feet will then have a raised toehold domain. A single-stranded fuel can bind to this raised domain, initiating displacement of the track and raising the foot. The fuel is designed to selectively raise the ‘back’ foot due to asymmetry within the system.

An earlier oxDNA study¹⁷⁸ revealed that the walker had a tendency to ‘overstep’, or bind to two non-adjacent sites (Fig. 9 (c)). This is disastrous for the walker, leaving both feet bound to the track without a free toehold to initiate foot-lifting. This tendency was observed even with tracks under moderate tension (~ 15 pN). Although tension could not prevent overstepping, increased disruption (fraying) of the front foot/track duplex hinted that recovery might be easier in the presence of tension, due to destabilisation of the overstepped state.

I now present evidence that tension does facilitate recovery from the overstepped state. I simulate toehold-free (blunt-ended) displacement of the track from the overstepped foot by a fuel molecule, as illustrated in Fig. 9 (d), both with and without a tension of 14.6 pN applied to the track. Langevin Dynamics simulations enhanced by FFS are used to estimate relative rates, and free-energy profiles of displacement are estimated using VMMC aided by US. Full methodological details are provided in the Supplementary Information. Kinetic simulations indicate that displacement is $\sim 5 \times 10^3$ faster with tension than without, and the free-energy profiles (Fig. 10) show that a difference of about $\Delta\Delta G_{\text{tension}} \approx 6.4k_B T$ develops between the two systems as displacement progresses.

When bound to two non-adjacent sites as in Fig. 9 (c), the walker tends to constrain the track and reduce its possible extension. Importantly, as individual base pairs between the forward edge of the front foot and the track are disrupted, the track is able to extend incrementally further (see Fig. 9 (d)). As a consequence, these base pairs break more easily than without tension – they have a higher tendency to be frayed prior to fuel binding, providing an effective toehold for displacement. Further, because base pairs with the fuel are more stable than with the track, displacement of the track is biased towards success (as evidenced by the slope at the start of displacement in Fig. 10 for the system under tension). Detailed inspection of the FFS results indicates that faster displacement is due to both easier binding

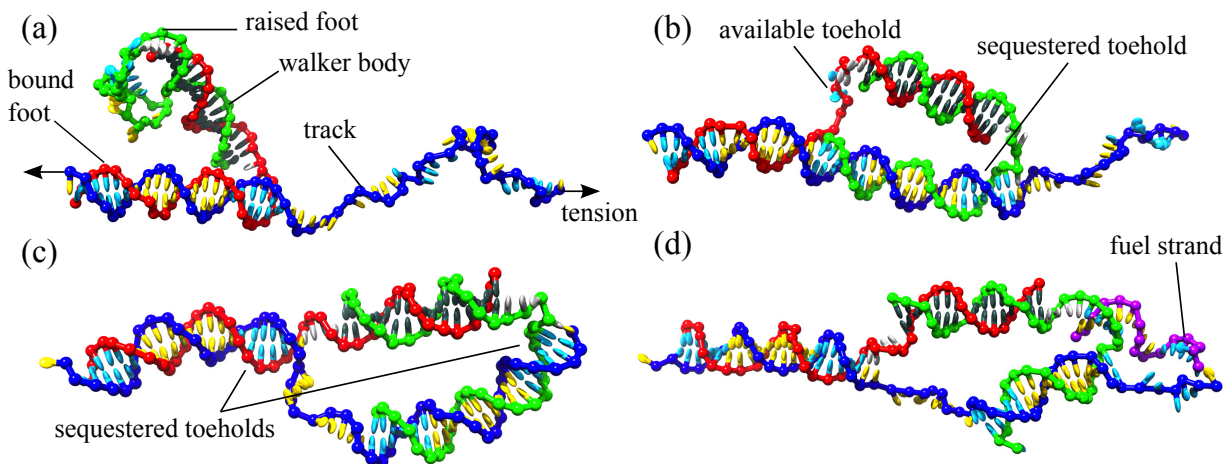


FIG. 9. States relevant to the operation of a two-footed DNA walker. The backbone of the track is coloured blue, the two feet red and green and the fuel purple. Bases are coloured according to their ‘domain’ – sky blue bases are toehold sequences, and yellow bases constitute the longer binding domains between track and foot. Dark green bases form the duplex that holds the two feet together. The system has an inherent asymmetry which allows the definition of forward and backward directions¹⁷⁸; in this figure, the forward direction is to the right. (a) Walker with one foot bound to the back site of a three-site track. (b) Walker bound to two adjacent sites on a three-site track, revealing a toehold for the fuel to raise the back foot. (c) Overstepped walker with sequestered toeholds. (d) Fuel displacing the track from the foot, prior to recovery of the walker from the overstepped state. In all figures, the track is subject to a tension of 14.6 pN in the horizontal direction.

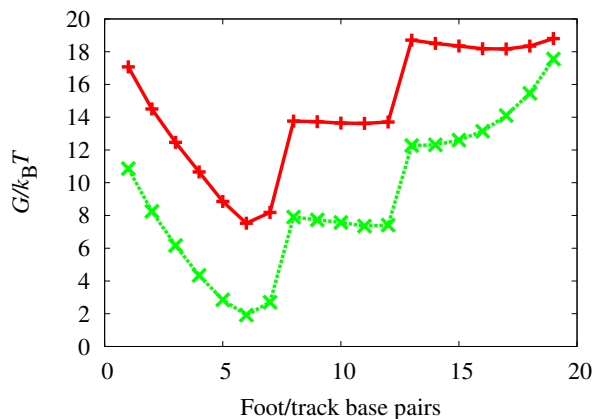


FIG. 10. Free-energy profile G for the raising of the front foot of an overstepped walker, given at least one base pair between an invading fuel strand and the foot. Data is shown for systems both with (green ‘x’ symbols) and without (red ‘+’ symbols) a tension of 14.6 pN applied the track. Free energies are measured relative to a reference state in which the fuel is yet to bind. Increasing displacement corresponds to reduced numbers of base pairs between foot and track - *i.e.*, moving from right to left on the graph. Large jumps at 7-8 and 12-13 are due to the repairing of mismatches by the invader; these mismatches are present by design to prevent enzymatic cleavage of the track. Statistical errors are similar in magnitude to the size of symbols; a more detailed discussion is given in the Supplementary Information.

and a higher subsequent probability of displacement success. If the thermodynamic results were used to estimate relative rates via $\exp(-\Delta\Delta G_{\text{tension}}/k_B T)$, a value of approximately 600 would be obtained. The statistical errors associated with the kinetic estimates in particular are substantial, so it is possible that the difference is

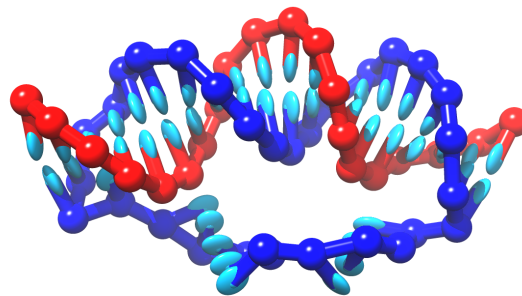


FIG. 11. Generating tension that will favour displacement in a “self contained” manner by using a short circular strand as the incumbent.

due to random error. However, it is also possible that the free-energy profile fails to highlight subtle kinetic effects, such as those that were observed in conventional displacement. Regardless, the two results clearly predict a substantial increase in walker recovery rate of $\sim 10^3$ or more under the application of moderate tension.

The fact that tension can aid walker recovery highlights the possibility of building contingency into nanodevice operation, thereby allowing for fail-safe behaviour. It also demonstrates the possibility of enhancing displacement through tension, an alternative way to modulate kinetics. In this case, tension is externally applied to the track; one possibility is to stretch the track between two points of an origami structure. One could generate tension in a more self-contained way by using circular substrates, as shown in Fig. 11; indeed, similar constructs have been studied experimentally^{179,180}. Here, a sufficiently long duplex section will apply an extensional

stress to a sufficiently short single-stranded section, and will experience a compression in response, leading to the bending shown in Fig. 11. Displacement rates in such a system could be modulated by secondary structure within, or binding to, the single-stranded loop of the substrate - this modulation would be freed from any constraints of the invader sequence.

V. DISCUSSION

DNA nanotechnology has enormous potential, but providing a solid theoretical underpinning is vital if it is to truly flourish. This understanding can be achieved through a combination of careful experimentation and modelling. Certain groups are now taking up the challenge of meticulously understanding the processes involved by carefully measuring important reactions in a variety of contexts^{31,64,85,86,89,90,92,93}. In this article I have discussed a coarse-grained model of DNA, oxDNA, that can complement these efforts. OxDNA is an attempt to incorporate the thermodynamics of DNA as parameterised by SantaLucia's nearest-neighbour model into a structural and mechanical framework consistent with current knowledge. It can then be used to study the behaviour of 'ideal' DNA, exploring the possibilities of certain motifs, testing whether new experimental observations are consistent with current understanding, and revealing which properties of DNA have an influence on certain phenomena.

I have reviewed a number of applications of oxDNA, demonstrating that it provides quantitative understanding of aspects of displacement processes and can offer qualitative insight into reaction mechanisms and novel motifs. In each case, a physically reasonable underlying cause for the observation in question was identified, such as stress that is generated or relieved during displacement. These effects should therefore be manifest in real DNA, rather than simply being artefacts of the model or simulation technique. Intriguing questions remain open, as there are many possible motifs available for study. For example, displacement reactions have recently been reported in the context of unconventional left-handed super-helices formed by conventional B-DNA domains in a complex pseudoknotted structure¹⁸¹ - such a system would be an ideal candidate for study with oxDNA. Other possibilities include studying the influence of single-stranded hairpins, which are frequently present both by accident and design, on hybridisation and displacement kinetics, and considering general properties of displacement cascades on surfaces⁹⁴.

oxDNA's strengths are its efficiency and good overall representation of the structural, mechanical and thermodynamic changes associated with short duplex formation. To achieve efficiency, however, the description of nucleotides is extremely simple and electrostatics in particular is treated in a basic fashion. Some properties, such as the opening of internal denaturation bubbles and

the structures of systems that are more complex than simple duplexes, are yet to be fully tested against experimental data. Characterising and improving these limitations will be the subject of further work.

oxDNA is parameterised to experimental data on the basic properties of DNA, but experimental results are not unequivocal. In particular, the typical state, stacking propensity and conformation of single strands are poorly understood (as discussed in Refs.^{137,138}), with some authors even finding evidence for structure formation when none would be expected from Watson-Crick base pairing¹⁸². Single strands have an enormous role in nanotechnological systems, not least as the initial state of the hybridisation process, which itself is not unambiguously understood. Particularly pertinent open questions relate to the temperature-dependence of hybridisation, as discussed in Ref.¹⁸³, and its behaviour near a surface⁹³. Mechanical properties of duplexes, and whether DNA can be described as a wormlike-chain at short length scales, are still the subject of debate^{184,185,186,187}. Resolving these fundamental issues would be extremely useful in nanotechnology and beyond. It is likely that, as further characterisation is performed, some of the assumptions inherent in the current understanding of DNA (and hence oxDNA) will have to be revisited.

In this article I have focussed on the application of oxDNA to small, active systems. oxDNA has also been used to study DNA in a range of other contexts, including large duplexes under applied stress¹⁸⁸, and self-assembly driven phase transitions^{189,190}. A modified version parameterised to describe RNA has recently been developed¹⁹¹. Although some progress has been made with improving the experimental protocols for constructing large structures^{85,86,89,90}, the assembly pathways and systematic ways to optimise them remain elusive. Modelling the assembly of larger structures with oxDNA is a current goal, but remains extremely challenging due to the large number of rare-event binding processes that must be observed. Further development and refinement of enhanced dynamic sampling techniques, such as FFS, would assist in this process. It may be that oxDNA can best be used to study smaller sub-structures, and that this information can then be incorporated into models at the level of secondary structure^{96,192} or whole binding domains^{87,88,193}.

¹W. Saenger, *Principles of Nucleic Acid Structure* (Springer-Verlag, New York, 1984).

²P.J. Hagerman, *Annu. Rev. Biophys. Biophys. Chem.* **17**, 265 (1988).

³J.B. Mills, E. Vacano and P.J. Hagerman, *J. Mol. Biol.* **285**, 245 (1999).

⁴M.C. Murphy, I. Rasnik, W. Chang, T.M. Lohman and T. Ha, *Biophys. J.* **86**, 2530 (2004).

⁵N.C. Seeman, *J. Theor. Biol.* **99**, 237 (1982).

⁶N.R. Kallenbach, R.I. Ma and N.C. Seeman, *Nature* **305**, 829 (1983).

⁷J. Zheng, J.J. Birktoft, Y. Chen, T. Wang, R. Sha, P.E. Constantinou, S.L. Ginell, C. Mao and N.C. Seeman, *Nature* **461**, 74 (2009).

- ⁸P.J. Paukstelis, J. Nowakowski, J.J. Birktoft and N.C. Seeman, *Chem. Biol.* **11**, 1119 (2004).
- ⁹H. Yan, S. Park, G. Finkelstein, J.H. Reif and T.H. LaBean, *Science* **301**, 1882 (2003).
- ¹⁰E. Winfree, F.R. Liu, L.A. Wenzler and N.C. Seeman, *Nature* **394**, 539 (1998).
- ¹¹J. Malo, J.C. Mitchell, C. Venien-Bryan, J.R. Harris, H. Wille, D.J. Sherrat and A.J. Turberfield, *Angew. Chem. Int. Ed.* **44**, 3057 (2005).
- ¹²F. Zhang, Y. Liu and H. Yan, *J. Am. Chem. Soc.* **135**, 7458 (2013).
- ¹³S. Biffi, R. Cerbino, F. Bomboi, E.M. Paraboschi, R. Asselta, F. Sciortino and T. Bellini, *Proc. Natl. Acad. Sci. U.S.A.* **110**, 15633 (2013).
- ¹⁴J. Chen and N.C. Seeman, *Nature* **350**, 631 (1991).
- ¹⁵Y. Zhang and N.C. Seeman, *J. Am. Chem. Soc.* **116**, 1661 (1994).
- ¹⁶R.P. Goodman, I.A.T. Sharp, C.F. Tardin, C.M. Erben, R.M. Berry, C.F. Schmidt and A.J. Turberfield, *Science* **310**, 1661 (2005).
- ¹⁷C.M. Erben, R.P. Goodman and A.J. Turberfield, *J. Am. Chem. Soc.* **129**, 6992 (2007).
- ¹⁸F.F. Andersen, B. Knudsen, C.L.P. Oliveira, R.F. Frohlich, D. Kruger, J. Bungert, M. Agbandje-McKenna, R. McKenna, J. Sissel, C. Veigaard, J. Koch, J.L. Rubinstein, B. Guldbbrandtsen, M.S. Hede, G. Karlsson, A.H. Andersen, J.S. Pedersen and B.R. Knudsen, *Nucl. Acids Res.* **36**, 1113 (2008).
- ¹⁹Y. Ke, L.L. Ong, W.M. Shih and P. Yin, *Science* **338**, 1177 (2012).
- ²⁰B. Wei, M. Dai and P. Yin, *Nature* **485**, 623 (2012).
- ²¹P.W.K. Rothmund, *Nature* **440**, 297 (2006).
- ²²S.M. Douglas, H. Dietz, T. Liedl, B. Högberg, F. Graf and W.M. Shih, *Nature* **459**, 414 (2009).
- ²³E.S. Andersen, M. Dong, M.M. Nielsen, K. Jahn, R. Subramani, W. Mamdough, M.M. Golas, B. Sander, H. Stark, C.L.P. Oliveira, J.S. Pedersen, V. Birkedal, F. Besenbacher, K.V. Gothelf and J. Kjems, *Nature* **459**, 73 (2009).
- ²⁴H. Dietz, S.M. Douglas and W.M. Shih, *Science* **325**, 725 (2009).
- ²⁵D. Han, S. Pal, J. Nangreave, Z. Deng, Y. Liu and H. Yan, *Science* **332**, 342 (2011).
- ²⁶S.Y. Park, A.K.R. Lytton-Jean, B. Lee, S. Weigand, G.C. Schatz and C.A. Mirkin, *Nature* **451**, 553 (2008).
- ²⁷F.A. Aldaye and H.F. Sleiman, *J. Am. Chem. Soc.* **129**, 13376 (2007).
- ²⁸J. Zimmermann, M.P. Cebulla, S. Monninghoff and G. von Kiedrowski, *Angew. Chem. Int. Ed.* **47**, 3626 (2008).
- ²⁹S.F.J. Wickham, J. Bath, Y. Katsuda, M. Endo, K. Hidaka, H. Sugiyama and A.J. Turberfield, *Nat. Nanotechnol.* **7**, 169 (2012).
- ³⁰B. Yurke and A. Mills, *Genetic Programming and Evolvable Machines* **4**, 111 (2003).
- ³¹D. Zhang and E. Winfree, *J. Am. Chem. Soc.* **131**, 17303 (2009).
- ³²N. Srinivas, T.E. Ouldrige, P. Šulc, J. Schaeffer, B. Yurke, A.A. Louis, J.P.K. Doye and E. Winfree, *Nucl. Acids Res.* **41**, 10641 (2013).
- ³³B. Yurke, A.J. Turberfield, A.P. Mills, F.C. Simmel and J. Neumann, *Nature* **406**, 605 (2000).
- ³⁴H. Yan, X.P. Zhang, Z.Y. Shen and N.C. Seeman, *Nature* **415**, 62 (2002).
- ³⁵R.P. Goodman, M. Heilemann, S.D. and C. M. Erben, A.N. Kapanidis and A.J. Turberfield, *Nat. Nanotechnol.* **3**, 93 (2008).
- ³⁶D. Han, S. Pal, Y. Liu and H. Yan, *Nat. Nanotechnol.* **5**, 712 (2010).
- ³⁷W.B. Sherman and N.C. Seeman, *Nano Lett.* (7), 1203 (2004).
- ³⁸J.S. Shin and N.A. Pierce, *J. Am. Chem. Soc.* **126**, 10834 (2004).
- ³⁹M. Liu, R. Hou, J. Cheng, I.Y. Loh, S. Sreelatha, J.N. Tey, J. Wei and Z. Wang, *ACS Nano* **8**, 1792 (2014).
- ⁴⁰J. Bath and A.J. Turberfield, *Nat. Nanotechnol.* **2**, 275 (2007).
- ⁴¹J. Bath, S.J. Green and A.J. Turberfield, *Angew. Chem. Int. Ed.* **117**, 4432 (2005).
- ⁴²J. Bath, S.J. Green, K.E. Allan and A.J. Turberfield, *Small* **5**, 1513 (2009).
- ⁴³S.F.J. Wickham, M. Endo, Y. Katsuda, K. Hidaka, J. Bath, H. Sugiyama and A.J. Turberfield, *Nat. Nanotechnol.* **6**, 166 (2011).
- ⁴⁴Y. Tian, Y. He, Y. Chen, P. Yin and C. Mao, *Angew. Chem. Int. Ed.* **44**, 4355 (2005).
- ⁴⁵K. Lund, A.J. Manzo, N. Dabby, N. Michelotti, A. Johnson-Buck, J. Nangreave, S. Taylor, R. Pei, M.N. Stojanovic, N.G. Walter, E. Winfree and H. Yan, *Nature* **465**, 206 (2010).
- ⁴⁶T.G. Cha, P. J. H. Chen, J. Salgado, X. Li, C. Mao and J.H. Choi, *Nat. Nanotechnol.* **9**, 39 (2014).
- ⁴⁷S.J. Green, J. Bath and A.J. Turberfield, *Phys. Rev. Lett.* **101**, 238101 (2008).
- ⁴⁸T. Omabegho, R. Sha and N.C. Seeman, *Science* **324**, 67 (2009).
- ⁴⁹S. Venkataraman, R.M. Dirks, P.W.K. Rothmund, E. Winfree and N.A. Pierce, *Nat. Nanotechnol.* **2**, 490 (2007).
- ⁵⁰R.A. Muscat, J. Bath and A.J. Turberfield, *Nano Lett.* **11**, 982 (2011).
- ⁵¹L.M. Adleman, *Science* **266**, 1021 (1994).
- ⁵²G. Seelig, D. Soloveichik, D.Y. Zhang and E. Winfree, *Science* **314**, 1585 (2006).
- ⁵³L. Qian and E. Winfree, *Science* **332**, 1196 (2011).
- ⁵⁴Y.J. Chen, N. Dalchau, N. Srinivas, A. Phillips, L. Cardelli, D. Soloveichik and G. Seelig, *Nat. Nanotechnol.* **8**, 755 (2013).
- ⁵⁵M.J. Berardi, W.M. Shih, S.C. Harrison and J.J. Chou, *Nature* **476**, 109 (2011).
- ⁵⁶D.N. Selmi, R.J. Adamson, H. Attrill, A.D. Goddard, A. Watts and A.J. Turberfield, *Nano Lett.* **11**, 657 (2011).
- ⁵⁷A. Kuzyk, R. Schreiber, Z. Fan, G. Pardatscher, E.M. Roller, A. Högele, F.C. Simmel, A.O. Govorov and T. Liedl, *Nature* **483**, 311 (2012).
- ⁵⁸P.K. Dutta, R. Varghese, J. Nangreave, S. Lin, H. Yan and Y. Liu, *J. Am. Chem. Soc.* **133**, 11985 (2011).
- ⁵⁹C.Y. Tseng and G. Zocchi, *J. Am. Chem. Soc.* **135**, 11879 (2013).
- ⁶⁰L. Minghui, J. Fu, C. Christian, Y. Yang, N.W. Woodbury, K.V. Gothelf, Y. Liu and H. Yan, *Nat. Commun.* **4**, 2127 (2013).
- ⁶¹J. Fu, M. Liu, Y. Liu, N.W. Woodbury and H. Yan, *J. Am. Chem. Soc.* **134**, 5516 (2012).
- ⁶²O.I. Wilner, Y. Weizmann, R. Gill, O. Lioubashevski, R. Freeman and I. Willner, *Nat. Nanotechnol.* **4**, 249 (2009).
- ⁶³J. Fu, Y.R. Yang, A. Johnson-Buck, M. Liu, Y. Liu, N.G. Walter, N.W. Woodbury and H. Yan, *Nat. Nanotechnol.* **9**, 531 (2014).
- ⁶⁴T.E. Tomov, R. Tsukanov, M. Liber, R. Masoud, N. Plavner and E. Nir, *J. Am. Chem. Soc.* **135**, 11935 (2013).
- ⁶⁵Y. Ke, S. Lindsay, Y. Chang, Y. Liu and H. Yan, *Science* **319**, 180 (2008).
- ⁶⁶H. Subramanian, B. Chakraborty, R. Sha and N. Seeman, *Nano Lett.* **11**, 910 (2011).
- ⁶⁷E. Pfitzner, C. Wachauf, F. Kilchherr, B. Pelz, W.M. Shih, M. Reif and H. Dietz, *Angew. Chem. Int. Ed.* **52**, 7766 (2013).
- ⁶⁸M. Endo, K. Tatsumi, K. Terushima, Y. Katsuda, K. Hidaka, Y. Harada and H. Sugiyama, *Angew. Chem. Int. Ed.* **124**, 8908 (2012).
- ⁶⁹N.D. Derr, B.S. Goodman, R. Jungmann, A.E. Lechziner, W.M. Shih and S.L. Reck-Peterson, *Science* **338**, 662 (2012).
- ⁷⁰S.M. Douglas, I. Bachelet and G.M. Church, *Science* **335**, 831 (2012).
- ⁷¹R. Crawford, C.M. Erben, J. Periz, L.M. Hall, T. Brown, A.J. Turberfield and A.N. Kapanidis, *Angew. Chem. Int. Ed.* **52**, 2284 (2013).
- ⁷²X. Liu, Y. Xu, T. Yu, C. Clifford, Y. Liu, H. Yan and Y. Chang, *Nano Lett.* **12**, 4254 (2012).
- ⁷³J. Li, H. Pei, B. Zhu, L. Liang, M. Wei, Y. He, N. Chen, D. Li, Q. Huang and C. Fan, *ACS Nano* **5**, 8783 (2011).
- ⁷⁴V.J. Schüller, S. Heidegger, N. Sandholzer, P.C. Nickels, N.A. Suhartha, S. Endres, C. Bourquin and T. Liedl, *ACS Nano* **5**, 9696 (2011).

- ⁷⁵A.S. Walsh, H. Yin, C.M. Erben, M.J.A. Wood and A.J. Turberfield, *ACS Nano* **5**, 5427 (2011).
- ⁷⁶H. Lee, A.K.R. Lytton-Jean, Y. Chen, K.T. Love, A.I. Park, E.D. Karagiannis, A. Sehgal, W. Querbes, C.S. Zurenko, M. Jayaraman, C.G. Peng, K. Charisse, A. Borodovsky, M. Manoharan, J.S. Donahoe, J. Truelove, M. Nahrendorf, R. Langer and D.G. Anderson, *Nat. Nanotechnol.* **7**, 389 (2012).
- ⁷⁷Q. Mei, X. Wei, F. Su, Y. Liu, C. Youngbull, R. Johnson, S. Lindsay, H. Yan and D. Meldrum, *Nano Lett.* **11**, 1477 (2011).
- ⁷⁸S. Surana, D. Bhatia and Y. Krishnan, *Methods* **64**, 94 (2013).
- ⁷⁹S.D. Perrault and W.M. Shih, *ACS Nano* **8**, 5132 (2014).
- ⁸⁰J. Mikkilä, A.P. Eskelinen, E.H. Niemelä, V. Linko, M.J. Frilander, P. Törmä and M.A. Kostiaainen, *Nano Lett.* **14**, 2196 (2014).
- ⁸¹Y. Amir, E. Ben-Ishay, D. Levner, S. Ittah, A. Abu-Horowitz and I. Bachalet, *Nat. Nanotechnol.* **9**, 353 (2014).
- ⁸²Y. He and D.R. Liu, *Nat. Nanotechnol.* **5**, 778 (2010).
- ⁸³M.L. McKee, P.J. Milnes, J. Bath, E. Stulz, R.K. O'Reilly and A.J. Turberfield, *J. Am. Chem. Soc.* **134**, 1446 (2012).
- ⁸⁴H. Gu, J. Chao, S. Xiao and N.C. Seeman, *Nature* **465**, 202 (2010).
- ⁸⁵J.P.J. Sobczak, T.G. Martin, T. Gerling and H. Dietz, *Science* **338**, 1458 (2012).
- ⁸⁶C. Myhrvold, M. Dai, P.A. Silver and P. Yin, *Nano Lett.* **13**, 4242 (2013).
- ⁸⁷A. Reinhardt and D. Frenkel, *Phys. Rev. Lett.* **112**, 238103 (2014).
- ⁸⁸J.M. Arbona, J. Elezgary and J.P. Aimé, *Europhys. Lett.* **100**, 28006 (2012).
- ⁸⁹Y. Ke, G. Bellot, N.V. Voigt, E. Fradkov and W.M. Shih, *Chem. Sci.* **3**, 2587 (2012).
- ⁹⁰T.G. Martin and H. Dietz, *Nat. Commun.* **3**, 1103 (2012).
- ⁹¹H. Chen, T.W. Weng, M.M.R. an Y. Cui, J. Irudayaraj and J.H. Choi, *J. Am. Chem. Soc.* **136**, 6995 (2014).
- ⁹²R. Tsukanov, T.E. Tomov, R. Masoud, H. Drory, N. Plavner, M. Liber and E. Nir, *J. Phys. Chem. B* **117**, 11932 (2013).
- ⁹³A. Johnson-Buck, J. Nangreave, S. Jiang, H. Yan and N.G. Walter, *Nano Lett.* **13**, 2754 (2013).
- ⁹⁴M. Teichmann, E. Kopperger and F.C. Simmel, *ACS Nano* (In Press).
- ⁹⁵J. SantaLucia, Jr. and D. Hicks, *Annu. Rev. Biophys. Biomol. Struct.* **33**, 415 (2004).
- ⁹⁶R.M. Dirks, J.S. Bois, J.M. Schaeffer, E. Winfree and N.A. Pierce, *SIAM Rev.* **29**, 65 (2007).
- ⁹⁷F. Oteri, M. Falconi, G. Chilemi, F.F. Andersen, C.L.P. Oliveira, J.S. Pedersen, B.R. Knudsen and A. Desideri, *J. Phys. Chem. C* **168**, 11519 (2011).
- ⁹⁸J. Yoo and A. Aksimentiev, *Proc. Natl. Acad. Sci. USA* **110**, 20099 (2013).
- ⁹⁹N.B. Becker and R. Everaers, *J. Chem. Phys.* **130**, 135102 (2009).
- ¹⁰⁰F. Lankaš, O. Gonzalez, L.M. Heffler, G. Stoll, M. Moakher and J.H. Maddocks, *Phys. Chem. Chem. Phys.* **11**, 10565 (2009).
- ¹⁰¹M. Sayar, B. Avşaroglu and A. Kabakçioğlu, *Phys. Rev. E* **81**, 041916 (2010).
- ¹⁰²A. Savel'yev and G.A. Papoian, *Proc. Natl. Acad. Sci. U.S.A.* **107**, 20340 (2010).
- ¹⁰³P.D. Dans, A. Zeida, M.R. Machado and S. Pantano, *J. Chem. Theory Comput.* **6**, 1711 (2010).
- ¹⁰⁴A. Morriss-Andrews, J. Rottler and S.S. Plotkin, *J. Chem. Phys.* **132**, 035105 (2010).
- ¹⁰⁵I.P. Kikot, A.V. Savin, E.A. Zubova, M.A. Mazo, E.B. Gusarova, L.I. Manevitch and A.V. Onufriev, *Biophysics* **56**, 387 (2011).
- ¹⁰⁶A.V. Savin, M.A. Mazo, I.P. Kikot, L.I. Manevitch and A.V. Onufriev, *Phys. Rev. B* **83**, 245406 (2011).
- ¹⁰⁷O. Gonzalez, D. Petkeviciūtė and J.H. Maddocks, *J. Chem. Phys.* **138**, 055102 (2013).
- ¹⁰⁸Y. He, M. Maciejczyk, S. Ołdziej, H.A. Scheraga and A. Liwo, *Phys. Rev. Lett.* **110**, 098101 (2013).
- ¹⁰⁹N.A. Kovaleva, I.P. Kikot, M.A. Mazo and E.A. Zubova, arXiv:1401.2770 (2014).
- ¹¹⁰N.B. Becker and R. Everaers, *Phys. Rev. E* **76**, 021923 (2007).
- ¹¹¹C. Maffeo, T.T.M. Ngo, T. Ha and A. Aksimentiev, *J. Chem. Theory Comput.* **10**, 2891 (2013).
- ¹¹²N. Korolev, D. Luo, A.P. Lyubartsev and L. Nordenskiöld, *Polymers* **6**, 1655 (2014).
- ¹¹³A. Naômé, A. Laaskonen and D.P. Vercauteren, *J. Chem. Theory Comput.* **10**, 3541 (2014).
- ¹¹⁴W.K. Olson, A.A. Gorin, X.J. Lu, L.M. Hock and V.B. Zhurkin, *Proc. Natl. Acad. Sci. U.S.A.* **95**, 11163 (1998).
- ¹¹⁵F. Trovato and V. Tozzini, *J. Phys. Chem. B* **112**, 13197 (2008).
- ¹¹⁶M.E. Johnson, T. Head-Gordon and A.A. Louis, *J. Chem. Phys.* **126**, 144509 (2007).
- ¹¹⁷C.W. Hsu, M. Fyta, G. Lakatos, S. Melchionha and E. Kaxiras, *J. Chem. Phys.* **137**, 105102 (2012).
- ¹¹⁸K. Drukker, G. Wu and G.C. Schatz, *J. Chem. Phys.* **114**, 579 (2001).
- ¹¹⁹M. Sales-Pardo, R. Guimera, A.A. Moreira, J. Widom and L. Amaral, *Phys. Rev. E* **71**, 051902 (2005).
- ¹²⁰F.W. Starr and F. Sciortino, *J. Phys.: Condens. Matter* **18**, 347 (2006).
- ¹²¹N.B. Tito and J.M. Stubbs, *Chem. Phys. Lett.* **485**, 354 (2010).
- ¹²²T.A. Knotts, IV, N. Rathore, D. Schwartz and J.J. de Pablo, *J. Chem. Phys.* **126** (084901) (2007).
- ¹²³E.J. Sambriski, D.C. Schwartz and J.J. de Pablo, *Biophys. J.* **96**, 1675 (2009).
- ¹²⁴D.M. Hinckley, G.S. Freeman, J.K. Whitmer and J.J. de Pablo, *J. Chem. Phys.* **139**, 144903 (2013).
- ¹²⁵C. Svaneborg, *Comput. Phys. Commun.* **183**, 1793 (2012).
- ¹²⁶M. Kenward and K.D. Dorfman, *J. Chem. Phys.* **130**, 095101 (2009).
- ¹²⁷M.C. Linak, R. Tourdot and K.D. Dorfman, *J. Chem. Phys.* **135**, 205120 (2011).
- ¹²⁸J.C. Araque, A.Z. Panagiotopoulos and M.A. Robert, *J. Chem. Phys.* **134**, 165103 (2011).
- ¹²⁹S. Niewieczerzał and M. Cieplak, *J. Phys.: Condens. Matter* **21**, 474221 (2009).
- ¹³⁰L.E. Edens, J.A. Brozik and D.J. Keller, *J. Phys. Chem. B* **116**, 14735 (2012).
- ¹³¹A.K. Dasanna, N. Destainville, J. Palmeri and M. Manghi, *Phys. Rev. E* **87**, 052703 (2013).
- ¹³²T. Cragolini, P. Derreumaux and S. Pasquali, *J. Phys. Chem. B* **117**, 8047 (2013).
- ¹³³K. Doi, T. Haga, H. Shintaku and S. Kawano, *Phil. Trans. R. Soc. A* **368**, 2615 (2010).
- ¹³⁴S.P. Mielke, N. Gronbeck-Jensen, V.V. Krishnan, W.H. Fink and C.J. Benham, *J. Chem. Phys.* **123**, 124911 (2005).
- ¹³⁵C. Knorowski, S. Burleigh and A. Travesset, *Phys. Rev. Lett.* **106**, 215501 (2011).
- ¹³⁶J.M. Arbona, J.P. Aimé and J. Elezgaray, *Phys. Rev. E* **86**, 051912 (2012).
- ¹³⁷T.E. Ouldridge, A.A. Louis and J.P.K. Doye, *J. Chem. Phys.* **134**, 085101 (2011).
- ¹³⁸T.E. Ouldridge, Ph.D. thesis, University of Oxford 2011 [Published as a book by Springer, Heidelberg, 2012].
- ¹³⁹P. Šulc, F. Romano, T.E. Ouldridge, L. Rovigatti, J.P.K. Doye and A.A. Louis, *J. Chem. Phys.* **137**, 135101 (2012).
- ¹⁴⁰J.H. Allen, E.T. Schoch and J.M. Stubbs, *J. Phys. Chem. B* **115**, 1720 (2011).
- ¹⁴¹T.R. Prytkova, I. Eryazici, B. Stepp, S. Nguyen and G.C. Schatz, *J. Phys. Chem. B* **114**, 2627 (2010).
- ¹⁴²M.J. Hoefert, E.J. Sambriski and J.J. de Pablo, *Soft Matter* **7**, 560 (2011).
- ¹⁴³T.J. Schmitt, B. Rogers and T.A. Knotts IV, *J. Chem. Phys.* **138**, 035102 (2013).
- ¹⁴⁴D. Hinckley, J.P. Lequieu and J.J. de Pablo, *J. Chem. Phys.* **141**, 035102 (2014).
- ¹⁴⁵F.B. Bombelli, F. Gambinossi, M. Lagi, D. Berti, G. Caminati, T. Brown, F. Sciortino, B. Norden and P. Baglioni, *J. Phys.*

- Chem. B **112**, 15283 (2008).
- ¹⁴⁶J.M. Arbona, J.P. Aimé and J. Elezgaray, *J. Chem. Phys.* **136**, 065102 (2012).
- ¹⁴⁷C. Svaneborg, H. Fellermann and S. Rasmussen, in *DNA Computing and Molecular Programming*, edited by D. Stefanovic and A. J. Turberfield (, , 2012), Vol. 7433, pp. 123–134.
- ¹⁴⁸T.E. Ouldrige, I.G. Johnston, A.A. Louis and J.P.K. Doye, *J. Chem. Phys.* **130**, 065101 (2009).
- ¹⁴⁹C. Svaneborg, H. Fellerman and S. Rasmussen, arxiv1210.6156 (2012).
- ¹⁵⁰T.I. Li, R. Sknepnek, R.J. Macfarlane, C.A. Mirkin and M.O. de la Cruz, *Nano Lett.* **12**, 2509 (2012).
- ¹⁵¹C. Hyeon and D. Thirumalai, *Proc. Natl. Acad. Sci. U.S.A.* **102**, 6789 (2005).
- ¹⁵²A. Cao and S.J. Chen, *Nucl. Acids Res.* **34**, 2634 (2006).
- ¹⁵³D. Jost and R. Everaers, *J. Chem. Phys.* **132**, 095101 (2010).
- ¹⁵⁴F. Ding, S. Sharma, P. Chalasani, V.V. Demidov, N.E. Broude and N.V. Dokholyan, *RNA* **14**, 1164 (2008).
- ¹⁵⁵S. Pasquali and P. Derreumaux, *The Journal of Physical Chemistry B* **114**, 11957 (2010).
- ¹⁵⁶A. Dickson, M. Maienschein-Cline, A. Tovo-Dwyer, J.R. Hammond and A.R. Dinner, *J. Chem. Theory Comput.* **7**, 2710 (2011).
- ¹⁵⁷N.A. Denesyuk and D. Thirumalai, *J. Phys. Chem. B* **117**, 4901 (2013).
- ¹⁵⁸M.A. Jonikas, R.J. Radmer, A. Laederach, R. Das, S. Pearlman, D. Herschlag and R.B. Altman, *RNA* **15**, 189 (2009).
- ¹⁵⁹R. Das and D. Baker, *Proc. Natl. Acad. Sci. U.S.A.* **104**, 14664 (2009).
- ¹⁶⁰M. Paliy, R. Melnik and B.A. Shapiro, *Phys. Biol.* **7**, 036001 (2010).
- ¹⁶¹Z. Xia, D.R. Bell, Y. Shi and P. Ren, *J. Phys. Chem. B* **117**, 3135 (2013).
- ¹⁶²S. Whitelam, E.H. Feng, M.F. Hagan and P.L. Geissler, *Soft Matter* **5**, 1251 (2009).
- ¹⁶³R.L. Davidchack, R. Handel and M.V. Tretyakov, *J. Chem. Phys.* **130**, 234101 (2009).
- ¹⁶⁴J. Russo, P. Tartaglia and F. Sciortino, *J. Chem. Phys.* **131**, 014504 (2009).
- ¹⁶⁵G.M. Torrie and J.P. Valleau, *J. Comp. Phys.* **23**, 187 (1977).
- ¹⁶⁶R.J. Allen, P.B. Warren and P.R. ten Wolde, *Phys. Rev. Lett.* **94**, 018104 (2005).
- ¹⁶⁷R.J. Allen, C. Valeriani and P.R. ten Wolde, *J. Phys.: Condens. Matter* **21**, 463102 (2009).
- ¹⁶⁸Q. Wang and B.M. Pettitt, *Biophys. J.* **106**, 1182 (2014).
- ¹⁶⁹T.E. Ouldrige, *J. Chem. Phys.* **137**, 144105 (2012).
- ¹⁷⁰R.R.F. Machinek, T.E. Ouldrige, N.E.C. Haley, J. Bath and A.J. Turberfield, *Nat. Commun.* In press. doi:NCOMMS6324
- ¹⁷¹A.J. Genot, D.Y. Zhang, J. Bath and A.J. Turberfield, *J. Am. Chem. Soc.* **133**, 2177 (2011).
- ¹⁷²D.Y. Zhang, S.X. Chen and P. Yin, *Nat. Chem.* **4**, 208 (2012).
- ¹⁷³Y.S. Jiang, S. Bhadra, B. Li and A.D. Ellington, *Angew. Chem. Int. Ed.* **126**, 1876 (2014).
- ¹⁷⁴Q. Li, G. Luan, Q. Guo and J. Liang, *Nucl. Acids Res.* **30**, e5 (2002).
- ¹⁷⁵D.Y. Zhang, S.X. Chen and Y. Peng, *Nat. Chem.* **4**, 208 (2012).
- ¹⁷⁶S.X. Chen, D.Y. Zhang and G. Seelig, *Nat. Chem.* **5**, 782 (2013).
- ¹⁷⁷P. Šulc, T.E. Ouldrige, F. Romano, J.P.K. Doye and A.A. Louis, *Nat. Comput.* pp. 1–13 (2013).
- ¹⁷⁸T.E. Ouldrige, R.L. Hoare, A.A. Louis, J.P.K. Doye, J. Bath and A.J. Turberfield, *ACS Nano* **7**, 2479 (2013).
- ¹⁷⁹H. Qu, Y. Wang, C.Y. Tseng and G. Zocchi, *Phys. Rev. X* **1**, 021008 (2011).
- ¹⁸⁰J. Wang, H. Qu and G. Zocchi, *Phys. Rev. E* **88**, 032712 (2013).
- ¹⁸¹Y. Li, C. Zhang, C. Tian and C. Mao, *Org. Biomol. Chem.* **12**, 2543 (2014).
- ¹⁸²J.R. Sikora, B. Rauzan, R. Stegemann and A. Deckert, *J. Phys. Chem. B* **117**, 8966 (2013).
- ¹⁸³T.E. Ouldrige, P. Šulc, F. Romano, J.P.K. Doye and A.A. Louis, *Nucl. Acids Res.* **41**, 8886 (2013).
- ¹⁸⁴P.A. Wiggins, T. van der Heijden, F. Moreno-Herrero, A. Spakowitz, R. Phillips, J. Widom, C. Dekker and P.C. Nelson, *Nat. Nanotechnol.* **1**, 137 (2006).
- ¹⁸⁵R. Vafabakhsh and T. Ha, *Science* **337**, 1097 (2012).
- ¹⁸⁶A. Vologodskii and M.D. Frank-Kamenetskii, *Nucl. Acids Res.* **41**, 6785 (2013).
- ¹⁸⁷A.K. Mazur and M. Maaloum, *Phys. Rev. Lett.* **112**, 068104 (2014).
- ¹⁸⁸J.P.K. Doye, T.E. Ouldrige, A.A. Louis, F. Romano, P. Šulc, C. Matek, B. Snodin, L. Rovigatti, J.S. Schreck, R.M. Harrison and W.P.J. Smith, *Phys. Chem. Chem. Phys.* **15**, 20395 (2013).
- ¹⁸⁹L. Rovigatti, F. Smalenburg, F. Romano and F. Sciortino, *ACS Nano* **8**, 3567 (2014).
- ¹⁹⁰L. Rovigatti, F. Bomboi and F. Sciortino, *J. Chem. Phys.* **140**, 154903 (2014).
- ¹⁹¹P. Šulc, F. Romano, T.E. Ouldrige, J.P.K. Doye and A.A. Louis, *J. Chem. Phys.* **140**, 235102 (2014).
- ¹⁹²J. Schaeffer, Ph.D. thesis, California Institute of Technology 2013.
- ¹⁹³A. Phillips and L. Cardelli, *J. R. Soc. Interface* **6**, S419 (2009).
- ¹⁹⁴S. Whitelam and P. L. Geissler, *J. Chem. Phys.* **127**, 154101 (2007).
- ¹⁹⁵S. Kumar, J. M. Rosenberg, D. Bouzida, R. H. Swendsen, and P. A. Kollman, *J. Comput. Chem.* **13**, 1011 (1992).
- ¹⁹⁶J. Lapham, J. P. Rife, P. B. Moore, and D. M. Crothers, *J. NMR* **10**, 252 (1997).

Appendix A: Simulation methods

Thermodynamic properties of model DNA are obtained by averaging over the Boltzmann distribution

$$\rho(\mathbf{r}^N, \mathbf{p}^N, \mathbf{q}^N, \mathbf{L}^N) \propto \exp(-\beta\mathcal{H}(\mathbf{r}^N, \mathbf{p}^N, \mathbf{q}^N, \mathbf{L}^N)), \quad (\text{S1})$$

where \mathcal{H} is the system Hamiltonian, \mathbf{r} and \mathbf{q} are positional and orientational degrees of freedom and \mathbf{p} and \mathbf{L} are linear and angular momenta. The momenta can be separately integrated analytically, and thus the relative probability of a configuration is given simply by $\exp(-\beta V(\mathbf{r}^N, \mathbf{q}^N))$. For oxDNA, thermodynamic averages are typically calculated using the Virtual Move Monte Carlo (VMMC) algorithm.^{162,194} Dynamical studies reported in this work use a Langevin Dynamics (LD) algorithm for rigid bodies,¹⁶³ which samples from the Boltzmann distribution and generates diffusive particle motion.

1. VMMC

VMMC^{162,194} is a cluster-based Monte Carlo technique that is particularly effective for dilute systems with strong, directional interactions such as oxDNA. Results reported in this work use the variant introduced in the appendix of Ref. 162. The algorithm involves attempting moves of particle clusters that are generated in a way that reflects potential energy gradients in the system, and accepting these attempted moves with a probability that ensures the system samples from the canonical ensemble. As clusters of strongly interacting particles move together, VMMC equilibrates oxDNA systems much more efficiently than traditional Monte Carlo algorithms.

‘Seed’ moves of a single particles are used to explore the energy gradients in a system and generate clusters. For all the VMMC simulations reported in this work, the seed moves were;

- rotation of a nucleotide about its backbone site, with the axis chosen from a uniform random distribution and the angle from a normal distribution with mean of zero and a standard deviation of 0.12 radians.
- translation of a nucleotide with the direction chosen from a uniform random distribution and the distance from a normal distribution with mean of zero and a standard deviation of 1.02 Å.

a. Umbrella Sampling

Many processes (such as the binding of two strands) are slow to equilibrate, despite the simplicity of oxDNA and the efficiency of VMMC as a simulation technique. Slow equilibration often arises when the system has multiple competing local minima of free energy, separated by large free-energy barriers. An artificial biasing weight $W(\mathbf{r}^N, \mathbf{q}^N)$ can be used to enhance equilibration by flattening these barriers.¹⁶⁵ This procedure, known as Umbrella Sampling (US), involves choosing $W(\mathbf{r}^N, \mathbf{q}^N)$ to favour the states of high free energy that must be crossed to pass between the free energy minima. The expectation of any variable A can be extracted from these biased simulations via

$$\langle A \rangle = \frac{\langle A(\mathbf{r}^N, \mathbf{q}^N)/W(\mathbf{r}^N, \mathbf{q}^N) \rangle_W}{\langle 1/W(\mathbf{r}^N, \mathbf{q}^N) \rangle_W}. \quad (\text{S2})$$

Here, $\langle \rangle_W$ indicates sampling from the biased ensemble in which states are visited with a probability proportional to $W(\mathbf{r}^N, \mathbf{q}^N) \exp(-\beta V(\mathbf{r}^N, \mathbf{q}^N))$. It is often helpful to define a (low-dimensional) order parameter $\psi(\mathbf{r}^N, \mathbf{q}^N)$ that describes the process in question, and to then define the bias $W(\psi)$ using this order parameter rather than through the individual coordinates.

b. The Weighted Histogram Analysis Method

Even with Umbrella Sampling it can be challenging to sample all relevant states of a system within a single simulation. It is sometimes advantageous to split the simulations into overlapping ‘windows’ of state space that can be separately equilibrated more easily. The data from the individual windows can be combined to give the statistical properties of the whole system by relating the windows using the overlapping regions. One systematic approach to achieve this is known as the ‘Weighted Histogram Analysis Method’ (WHAM).¹⁹⁵ To use the WHAM algorithm, one must supply

- $W^i(\psi)$, the biasing potential used in window i .

- $\rho^i(\psi)$, the normalised distribution measured during simulation window i .
- n^i , the total number of VMMC steps taken over all simulations in window i .

The WHAM algorithm takes these inputs and iteratively estimates the overall distribution $\rho(\psi)$ and the dimensionless free-energy of window i (F_i), via the equations

$$\rho^i(\psi) = \frac{\sum_i \rho^i(\psi) n^i}{\sum_i n^i \exp(F_i) W^i(\psi)},$$

$$\rho(\psi) = \frac{\rho^i(\psi)}{\sum_\psi \rho^i(\psi)}, \quad (\text{S3})$$

$$\exp(-F^i) = \sum_\psi W^i(\psi) \rho(\psi).$$

From an initial (trivial) choice of F_i , the measured data can be used to iterate these equations until convergence, resulting in an overall estimate of the unbiased occupancy of individual states, $\rho(\psi)$.

2. Langevin Dynamics

LD allows Newton’s equations of motion for the particles that are explicit in the model to be augmented with random and dissipative forces due to an implicit solvent. These forces are chosen so that particles move diffusively and the system samples from the Boltzmann distribution. The kinetic results reported in this work were obtained using the quaternion-based algorithm for rigid bodies of Davidchack *et al.*¹⁶³ Other work on oxDNA has been performed with an Andersen-like thermostat.¹⁶⁴

To use the LD algorithm, a nucleotide mass (which is taken as $m = 315.75$ Da for all nucleotides) and a moment of inertia tensor (we treat the nucleotides as spherical with a moment of inertia 31.586 Da nm²) are required.¹³⁸ The drag forces experienced by a particle must also be related to its generalised momenta via a friction tensor. We ignore the complexity of hydrodynamic coupling between particles. For simplicity, we treat each nucleotide’s interaction with the solvent as spherically symmetric which means that only linear and rotational damping coefficients γ and Γ remain as independent quantities. The investigations reported in this paper use values of $\gamma = 0.59$ ps⁻¹ and $\Gamma = 1.76$ ps⁻¹. These values result in diffusion coefficients of $D_{\text{sim}} = 1.91 \times 10^{-9}$ m²s⁻¹ for a 14 base-pair duplex, higher than experimental measurements of $D_{\text{exp}} = 1.19 \times 10^{-10}$ m²s⁻¹.¹⁹⁶ Accelerating diffusion in this manner allows simulations to explore more complex processes for a given CPU time. Our group has previously shown¹⁸³ that increased friction coefficients have almost no qualitative consequences for hybridization pathways in oxDNA, only an overall reduction in the reaction rate. LD Simulations in this work use an integration time step of 8.55 fs, which has been previously shown to reproduce the energies and kinetics obtained with shorter time steps for oxDNA.¹³⁸

In the studies reported in this work, I compare the measured rates of similar processes; typically, displacement rates as certain system parameters are changed. For such comparisons, the effects of the choice of dynamical method should be approximately the same in each case, meaning that relative rates should be reasonably insensitive to the details of the dynamical algorithm. Furthermore, the numerical results are made meaningful by identifying the physically reasonable factors that lead to them, rather than just reporting the results in isolation.

a. Forward flux sampling

‘Brute force’ LD simulations are often not efficient enough to sample rare transitions accurately. Forward Flux Sampling (FFS) can be used to enhance the calculation of the flux between two local free-energy minima, and improve sampling from the trajectories that link the two regions (*reactive trajectories*).^{166,167} Here I outline the general method; our specific implementation is detailed in Section C.

Firstly I define the term ‘flux’. Let A and B be two non-overlapping regions of phase space. The flux from A to B is defined in the following way.

For an infinitely long simulation, the flux of trajectories from A to B is $\Phi_{AB} = N_{AB}/(\tau f_A)$, where N_{AB} is the number of times the simulation leaves A and then reaches B without first returning to A , τ is the total simulation time and f_A is the fraction of simulation time during which the system visited state A more recently than state B .

The concept of flux generalises a transition rate for processes that are not absolutely instantaneous.

To use FFS, a one-dimensional discrete order parameter Q is required so that non-intersecting interfaces λ_{n-1}^n exist between consecutive values of Q . The lowest value of Q , $Q = -2$, defines state A , and the highest value $Q = Q_{\max}$ state B . Initially, a simulation is performed in the vicinity of $Q = -2$, and the flux of trajectories from $Q = -2$ to $Q = 0$ is measured (in effect, one counts the trajectories that cross the surface λ_{-1}^0 for the first time since leaving $Q = -2$). I choose to define the lowest value of Q as $Q = -2$ because the algorithm is distinct for values of $Q > 0$.

The total flux of trajectories from A to B then follows as the flux across λ_{-1}^0 from $Q = -2$, multiplied by the conditional probability that these trajectories subsequently cross the interface $\lambda_{Q_{\max}-1}^{Q_{\max}}$ to reach $Q = Q_{\max}$ instead of returning to $Q = -2$, $P(\lambda_{Q_{\max}-1}^{Q_{\max}}|\lambda_{-1}^0)$. This probability can itself be expressed as a product of the success probabilities associated with reaching the next interface (rather than returning to $Q = -2$) for each in-

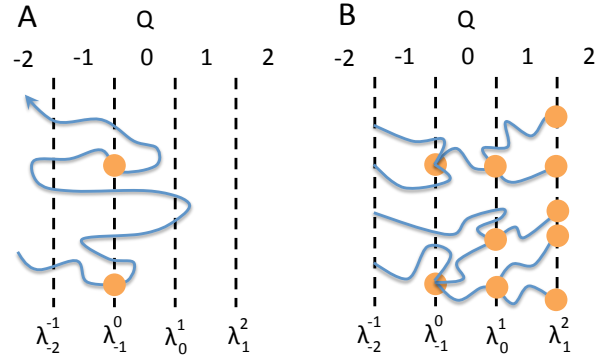


FIG. S12. Schematic illustrations of FFS. An order parameter Q is defined with interfaces λ separating distinct value of Q . We are interested in measuring the flux from $Q = -2$ to $Q = 2$ in this example. A) The initial measurement of flux across the interface λ_{-1}^0 . Orange dots indicate the crossings that contribute to the flux, and also the states used to launch subsequent stages of simulation. B) Direct FFS involves randomly launching many trajectories from the interface λ_{-1}^0 , and measuring the probability of reaching λ_0^1 before returning to λ_{-2}^{-1} . This procedure is then repeated for successive interfaces, resulting in branched trajectories. Reprinted by permission from T. E. Ouldridge *et al.*, DNA hybridization kinetics: zipping, internal displacement and sequence dependence, Nucleic Acids Research 41:8886-8895. Copyright (2013) Oxford University Press.¹⁸³

Strand	Sequence (5'-3')
Substrate	GAC ATG GAG ACG TAG GGT ATT GAA TGA GGG
Incumbent	TCC CTC ATT CAA TAC CCT ACG
Invader	CC CTC ATT CAA TAC CCT ACG

TABLE S1. Sequences used to simulate zero-toehold displacement. Italic regions indicate the displacement domain.

termediate case, $P(\lambda_{Q-1}^Q|\lambda_{Q-2}^{Q-1})$:

$$P(\lambda_{Q_{\max}-1}^{Q_{\max}}|\lambda_{-1}^0) = \prod_{Q=1}^{Q_{\max}} P(\lambda_{Q-1}^Q|\lambda_{Q-2}^{Q-1}). \quad (\text{S4})$$

In this work, the ‘direct’ FFS approach was used to calculate the product in Equation S4. In this method, a flux simulation is run to calculate the flux from $Q = -2$ to $Q = 0$, and generate states at the λ_{-1}^0 interface. These states are used as starting points for estimating $P(\lambda_0^1|\lambda_{-1}^0)$. The process is then iterated for subsequent interfaces, using the successes from the previous stage as initial configurations for the next. The branched trajectories obtained sample from the distribution of reactive trajectories. The procedure is illustrated schematically in Fig. S12.

b. Error estimation

In the initial work on FFS, the authors suggested calculating statistical error by treating each stage of the

Strand	Sequence (5' - 3')								
Track (3 sites)	C	AGCATC	C [^] TTTCAGC [^] TTTC	AGCATC	C [^] TTTCAGC [^] TTTC	AGCATC	C [^] TTTCAGC [^] TTTC	AGCATC	C
Walker 1			GTATTATCGTTAGTCT	tttt	GATGCT	GAGGCTGA [^] GG	GATGCT		
Walker 2			AGACTAACGATAATAC	tttt	GATGCT	GAGGCTGA [^] GG	GATGCT		
Fuel					CCTCAGCCTC	AGCATC			

TABLE S2. Sequences used for simulating the DNA walker. Complementary regions are highlighted in the same colour (corresponding to the colours used for the base sites in Fig. 9 of the main text). The toehold domains are highlighted in blue, and the longer binding domains in yellow. The duplex that holds the walker together is shown in green. Circumflexes indicate mismatched bases between the foot and track (which prevent the track from being cleaved by nicking enzymes in experiment, and also favour foot-lifting by the fuel). Although the fuel can in principle bind to either toehold of both walker strands, only the 5' end will naturally lead to displacement.

simulation as independent attempt to estimate a probability $P(\lambda_i^{i+1}|\lambda_{i-1}^i)$ through a number of independent trials. Such an approach gives the variance in the measured value of $P(\lambda_i^{i+1}|\lambda_{i-1}^i)$ as

$$\sigma_i^2 = P(\lambda_i^{i+1}|\lambda_{i-1}^i)(1 - P(\lambda_i^{i+1}|\lambda_{i-1}^i))/N_i, \quad (\text{S5})$$

where N_i is the number of trials launched from interface i . The overall variance in the flux measurement would then follow by summing the individual variances from each stage.

Our group followed this approach in Refs. 178 and 32. However, this method underestimates the true variability of the final result, as it assumes that the initial configurations at each interface are a truly representative ensemble. In some cases, particularly when bottlenecks appear in the process, this assumption can be poorly justified. For example, analysis of the simulation results for the zero-toehold displacement presented in Ref. 32 showed that only a few of the initial configurations obtained at the λ_{-1}^0 interface subsequently spawned trajectories that led to complete displacement, raising the possibility that the true uncertainty in the result is much higher than suggested.

An alternative approach is to estimate statistical errors by running a number of completely separate FFS protocols and comparing the independent estimates of the overall flux. I have used this procedure for the simulations of walker recovery presented in this work. To check the reliability of our earlier result on TMSD, I also present data for zero-toehold displacement obtained using this approach in the main text. Overall, although error estimates may have been too small, the physical conclusions drawn from earlier work are robust.

Appendix B: Systems

1. Zero-toehold displacement

Simulations of zero-toehold displacement used the same setup as Ref. 32. Simulations involved one invader, one substrate and one incumbent in a periodic cubic cell of 1.67×10^{-20} l (litres), at a temperature of $T = 298.15$ K. Table S1 contains strand sequences. As

in the original work,³² the sequence-independent version of oxDNA was used, and only base pairs native to the initial incumbent/substrate and final invader/substrate duplexes were assigned non-zero binding strength. This simplification eliminates the metastable misbonded configurations, which can hamper FFS without significantly affecting system behaviour.³² The sequence-independent parameterisation of oxDNA can simplify results as it shows only the generic behaviour of DNA, rather than sequence-specific effects.

Appendix C: Simulation protocols

1. Overstepped walker recovery

Walker simulations involved the two strands that constitute the walker itself, a track containing three binding sites with one extra base at either end to limit the effects of truncating the track, and a fuel strand in a periodic cubic cell of 7.73×10^{-20} l. Table S2 displays the sequences. A temperature of 310 K was used, close to experimental conditions.⁴² For simulations involving tension, a constant force of 14.6 pN was applied to the backbone sites at either end of the track. Consistent with earlier work on the walker using oxDNA,¹⁷⁸ the sequence-independent parameterisation of oxDNA was used. To simplify sampling, only expected interstrand bonds (*i.e.*, those intended in the design) were assigned non-zero binding strength, although any intrastrand base-pairing was allowed.

2. Kinetic simulations of blunt-ended displacement

I performed 10 completely independent implementations of FFS to estimate displacement rate for zero-base toeholds in oxDNA. In each case, I measured the flux from the initial state (incumbent/substrate duplex, separate invader) to the final state (invader/substrate duplex, separate incumbent) using the order parameter outlined in Table S3. The order parameter involves the number of *nearly formed* base pairs; a base pair is defined as nearly formed if and only if the following criteria hold.

Order parameter Q	Distance d/nm	Nearly-formed base pairs n	Number of base pairs A with $E < -2.98 \text{ kcal mol}^{-1}$	Number of base pairs B with $E < -2.98 \text{ kcal mol}^{-1}$	Distance d_2/nm
-2	$d > 5.11$	\sim	\sim	\sim	\sim
-1	$5.11 > d > 3.41$	\sim	\sim	\sim	\sim
0	$3.41 > d > 2.56$	\sim	\sim	\sim	\sim
1	$2.56 > d > 1.70$	\sim	\sim	\sim	\sim
2	$1.70 > d > 0.852$	\sim	\sim	\sim	\sim
3	$0.852 > d$	0	0	\sim	\sim
4	\sim	1	0	\sim	\sim
5	\sim	\sim	$A = 1$	\sim	\sim
6	\sim	\sim	\sim	$1 < B < 4$	\sim
7	\sim	\sim	\sim	$4 < B < 20$ or $(B = 20 \ \& \ d_2 < 2.56)$	\sim
8	\sim	\sim	\sim	$B = 20$	$d_2 \geq 2.56$

TABLE S3. Order parameter definition for FFS simulations of blunt-ended displacement. d and d_2 are minimum distances within certain sets of pairs of bases, measured as the separation of hydrogen-bonding sites of a pair. ‘‘Nearly-formed’’ base pairs are defined in the text. The pairs of bases considered for d , n and A are only the 3 base pairs at either end of the intended invader/substrate duplex. B includes *all* intended base pairs in the invader/substrate duplex. d_2 includes all base pairs in the original incumbent/substrate duplex. ‘‘ \sim ’’ indicates that no additional restriction is placed on this collective degree of freedom that is not covered by other explicitly stated requirements.

Number of replicas	10
Number of simulations per replica for flux across λ_{-1}^0	10
Initialisation time per simulation /ns	85.5
Total crossings of λ_{-1}^0 (total time taken/ μs)	10000 181
Average flux across $\lambda_{-1}^0/\mu\text{s}^{-1}$	55.2
Target interface	Total states loaded/successes
λ_0^1	100000/41957
λ_1^2	100000/42826
λ_2^3	100000/21010
λ_3^4	100000/ 14469
λ_4^5	800000/41467
λ_5^6	400000/12297
λ_6^7	200000/2797
λ_7^8	5000/267
Overall flux to full displacement/ s^{-1} (individual replica estimates)	0.0149 0.026 0.00482 0.0356 0.000975 0.00362 0.0220 0.0200 0.00475 0.139

TABLE S4. Simulation details and data obtained from FFS simulations of blunt-ended displacement.

- The separation of hydrogen bonding sites is $\leq 0.85 \text{ nm}$.
- The hydrogen-bonding potential consists of a separation dependent factor multiplied by a number of modulating angular factors. At most one of these factors that contributes multiplicatively to the hydrogen-bonding energy is zero.

Physically, these conditions mean that the bases are close and fairly well aligned, but not forming a strong base pair.

In Ref. 32, it was observed that all successful instances of blunt-ended displacement began with attachment at one of the three bases at either end of the displacement domain. In this work, I use an order parameter that assumes a pathway in which displacement begins with attachment at either end of the displacement domain. This enables more efficient sampling of this dominant pathway at the cost of less efficient sampling of alternatives, which are assumed to be irrelevant.

For each of the 10 independent FFS implementations, I ran 10 simulations to measure the initial flux. In each case, 100 states at the interface λ_{-1}^0 were collected, giving 10000 in total. All simulations were initialised in the same state, but then separately thermalised before flux measurement.

For each subsequent interface, a large number of trajectories were launched and those that reached the next interface before returning to $Q = -2$ were saved. The number of attempts made at each interface are given in Table S4.

3. Kinetic simulations of walker recovery

The procedure for kinetic simulations of walker recovery by fuel invasion was generally similar to that outlined

Order parameter Q	Distance d/nm	Nearly-formed base pairs n	Number of base pairs A with $E < E_A$	Number of base pairs B with $E < E_B$
-2	$d > 6.81$	\sim	\sim	\sim
-1	$6.81 > d > 5.11$	\sim	\sim	\sim
0	$5.11 > d > 4.26$	\sim	\sim	\sim
1	$4.26 > d > 3.41$	\sim	\sim	\sim
2	$3.41 > d > 2.56$	\sim	\sim	\sim
3	$2.56 > d > 1.70$	\sim	\sim	\sim
4	$1.70 > d > 0.852$	\sim	\sim	\sim
5	$0.852 > d$	0	0	0
6	\sim	1	0	0
7	\sim	\sim	$(A \geq 1 \ \& \ B = 0)$ or $(A = 1 \ \& \ B = 1)$	
8	\sim	\sim	$(A \geq 2 \ \& \ B = 1)$ or $(A = 2 \ \& \ B = 2)$	
9	\sim	\sim	$A \geq 3$	$4 > B \geq 2$
10	\sim	\sim	\sim	$16 > B \geq 4$
11	\sim	\sim	\sim	16

TABLE S5. Order parameter definition for FFS simulations of walker recovery by fuel displacement. d is the minimum distance between bases that are intended to form base pairs in the final invader/substrate duplex, measured as the separation of hydrogen-bonding sites. ‘‘Nearly-formed’’ base pairs are defined in the text. All base-pairing contributions to the order parameter include only those base pairs that are intended to be present in the final invader/substrate duplex. $E_A = -1.43 \text{ kcal mol}^{-1}$ and $E_B = -1.79 \text{ kcal mol}^{-1}$. ‘‘ \sim ’’ indicates that no additional restriction is placed on this collective degree of freedom that is not covered by other explicitly stated requirements.

in Section C 2 for blunt-ended displacement. Order parameter definitions and simulation details are presented in Tables S5 and S6 (note that, in this case, I make no assumptions about where initial attachment occurs).

In simulations, the effective concentration of the walker and fuel are much higher than typical of experiment. As a result, the ratio of time spent whilst displacement is in progress to time spent waiting for fuel-binding is much higher. It is possible, therefore, that in our system recovery of the foot is not an effectively instantaneous process compared to the lifetime of the overstepped state, as would be expected in experiment. To avoid this confusion, I did not include time spent with the fuel partially bound to the walker in our estimate of the initial flux – a simple way to do this was to restart flux simulations if they reached the interface λ_6^7 in Table S5 (the point at which the fuel starts to form base pairs with the walker), rather than waiting until λ_{10}^{11} before doing so. The overall procedure is in fact equivalent to measuring the flux from $Q = -2$ to $Q = 7$, and then the subsequent probability of going on from $Q = 7$ to $Q = 11$ rather than back to $Q = -2$.

The fuel is only 16 bases long, and hence cannot fully displace the track from the foot – the final six base pairs must break spontaneously. In this work I use the rate at which this maximally displaced state is reached as a proxy for the rate of recovery (foot-lifting). From the known behaviour of toehold-mediated strand displacement, one would expect detachment of this region of six base pairs to be faster than reverse-displacement of the fuel by the track, a process that would be even slower than normal due to the need to overcome two mismatches.^{32,170} Consequently the probability of recovery once the six-base-pair state is reached should be high, justifying the approximation in this work.

4. Thermodynamic simulations of walker recovery

I performed thermodynamic simulations of walker recovery using VMMC aided by US and WHAM. I divided state space into three overlapping ‘windows’, and ran 10 simulations confined to each window. The order parameter $\psi(\mathbf{r}^N, \mathbf{q}^N)$ used to define the umbrella potential was three-dimensional:

- ψ_1 : the number of base pairs between the overstepped foot and the track with a base-pairing interaction more negative than $-0.596 \text{ kcal mol}^{-1}$.
- ψ_2 : the number of base pairs between the overstepped foot and the fuel with a base-pairing interaction more negative than $-0.596 \text{ kcal mol}^{-1}$.
- ψ_3 : a measure of the proximity of the fuel and the overstepped walker foot, measured as the minimum distance d between hydrogen-bonding sites of bases in the fuel and foot domain to which it binds. For historical reasons, in the simulations without tension this distance d was only calculated using base pairs that can form in the intended foot-track duplex; in the simulations with fuel, it was calculated using any pair of bases in the two domains. Although this leads to different sampling behaviour, it does not invalidate the schemes. 4 states of ψ_3 were used:

- $\psi_3 = 0$: $d > 8.52 \text{ nm}$.
- $\psi_3 = 1$: $8.52 \text{ nm} \geq d > 4.26 \text{ nm}$.
- $\psi_3 = 2$: $4.26 \text{ nm} \geq d > 2.56 \text{ nm}$.
- $\psi_3 = 3$: $2.56 \text{ nm} \geq d$.

System	With tension	Without tension
Number of replicas	10	10
Number of simulations per replica for flux across λ_{-1}^0	10	10
Initialisation time per simulation / μ s	2.565	2.565
Total crossings of λ_{-1}^0 (total time taken/ μ s)	2557 94.2	3090 126
Average flux across λ_{-1}^0/μ s $^{-1}$	27.1	24.5
Target interface	Total states	loaded/successes
λ_0^1	40000/18156	40000/17850
λ_1^2	39803/21181	38975/20341
λ_2^3	37600/21154	39947/22017
λ_3^4	40000/22095	40000/21060
λ_4^5	71200/20636	76000/18448
λ_5^6	40000/9708	80000/11296
λ_6^7	99000/3353	200000/1744
λ_7^8	37939/5869	200000/5878
λ_8^9	20000/3981	160000/2629
λ_9^{10}	5000/2137	30000/5105
λ_{10}^{11}	1880/909	3880/773
Overall flux to full displacement/ s^{-1} (individual replica estimates)	135 37.1 45.5 32.3 58.1 7.96 1.49 47.9 18.3 11.3	0.00438 0.00340 0.0332 0.00131 0.00384 0.00492 0.00987 0.01345 0.00376 0.00167

TABLE S6. Simulation details and data obtained from FFS simulations of walker recovery.

The biasing weights used for each simulation window are outlined in Tables S7, S8, S9, S10, S11 and S12. For a given window, systems were initialised in the same state and then thermalised prior to data collection. 10^9 and 10^{10} VMMC steps were used for initialisation and data collection for the first window in each case; 2×10^9 and 2×10^{10} were used for the second and third windows for

both systems. Data from distinct windows were combined using the WHAM algorithm.¹⁹⁵

Appendix D: Results and error analysis

1. Kinetic simulations of blunt-ended displacement

The results for the 10 independent FFS implementations are presented in Table S4. As is evident, the random error is substantial (and much larger than would be estimated from the simple argument outlined in Section A 2). Averaging the results and taking a standard error on the mean would lead to an estimate of $0.027 \pm 0.013 \text{ s}^{-1}$, significantly higher than reported in Ref. 32 (0.005 s^{-1}). The new result, however, is not less consistent with the experimental data. The previous result suggested that zero-base toehold was slower relative to a six-base toehold in oxDNA than in reality. The new measurements also have no consequences for the physical interpretation provided in Ref. 32, which was not based on the behaviour of the zero-base toehold itself but on observations related to why longer toeholds (which were sampled more reliably) had a high probability of detaching before displacement could proceed.

2. Kinetic simulations of walker recovery

The results for the 10 independent FFS implementations of walker recovery with and without tension applied to the track are presented in Table S6. Once again, the random errors are substantial due to the difficulty of measuring such slow processes with large systems, but the overall difference between systems with and without tension is clear.

3. Thermodynamic simulations of walker recovery

The overall thermodynamic data for simulations of walker recovery are presented in the main text. The random error can be estimated by grouping the data into 10 independent sets (each one containing one of the independent simulations from each window), and running the WHAM algorithm on each one separately. The results of such a procedure are shown in Fig. S13 – the standard error on the mean for the free-energy relative to the unbound state is typically $\sim 0.2 - 0.3 k_B T$.

ψ_1	$\psi_2 = 0, \psi_3 =$				$\psi_3 = 3, \psi_2 =$															
	0	1	2	3	1	2	3	4	5	6	7	8	9	10	11	12	13	14	15	16
0	0	0	0	0	0	0	0	0	0	0	0	0	0	0	0	0	0	0	0	0
1	1	20	500	4000	1.2×10^8	1.2×10^8	1.2×10^8	0	0	0	0	0	0	0	0	0	0	0	0	0
2	1	20	500	4000	1.2×10^8	1.2×10^8	1.2×10^8	0	0	0	0	0	0	0	0	0	0	0	0	0
3	1	20	500	4000	1.2×10^8	1.2×10^8	1.2×10^8	0	0	0	0	0	0	0	0	0	0	0	0	0
4	1	20	500	4000	1.2×10^8	1.2×10^8	1.2×10^8	0	0	0	0	0	0	0	0	0	0	0	0	0
5	1	20	500	4000	1.2×10^8	1.2×10^8	1.2×10^8	0	0	0	0	0	0	0	0	0	0	0	0	0
6	1	20	500	4000	1.2×10^8	1.2×10^8	1.2×10^8	0	0	0	0	0	0	0	0	0	0	0	0	0
7	1	20	500	4000	1.2×10^8	1.2×10^8	1.2×10^8	0	0	0	0	0	0	0	0	0	0	0	0	0
8	1	20	500	4000	1.2×10^8	1.2×10^8	1.2×10^8	0	0	0	0	0	0	0	0	0	0	0	0	0
9	1	20	500	4000	1.2×10^8	1.2×10^8	1.2×10^8	0	0	0	0	0	0	0	0	0	0	0	0	0
10	1	20	500	4000	1.2×10^8	1.2×10^8	1.2×10^8	0	0	0	0	0	0	0	0	0	0	0	0	0
11	1	20	500	4000	1.2×10^8	1.2×10^8	1.2×10^8	0	0	0	0	0	0	0	0	0	0	0	0	0
12	1	20	500	4000	1.2×10^8	1.2×10^8	1.2×10^8	0	0	0	0	0	0	0	0	0	0	0	0	0
13	1	20	500	4000	1.2×10^8	1.2×10^8	1.2×10^8	0	0	0	0	0	0	0	0	0	0	0	0	0
14	1	20	500	4000	1.2×10^8	1.2×10^8	1.2×10^8	0	0	0	0	0	0	0	0	0	0	0	0	0
15	1	20	500	4000	1.2×10^8	1.2×10^8	1.2×10^8	0	0	0	0	0	0	0	0	0	0	0	0	0
16	1	20	500	4000	1.2×10^8	1.2×10^8	1.2×10^8	0	0	0	0	0	0	0	0	0	0	0	0	0
17	1	20	500	4000	1.2×10^8	1.2×10^8	1.2×10^8	0	0	0	0	0	0	0	0	0	0	0	0	0
18	1	20	500	4000	1.2×10^8	1.2×10^8	1.2×10^8	0	0	0	0	0	0	0	0	0	0	0	0	0
19	1	20	500	4000	1.2×10^8	1.2×10^8	1.2×10^8	0	0	0	0	0	0	0	0	0	0	0	0	0
20	1	20	500	4000	1.2×10^8	1.2×10^8	1.2×10^8	0	0	0	0	0	0	0	0	0	0	0	0	0

TABLE S7. Biasing potential $W(\psi)$ for window 1 of an overstepped walker without tension, with $\psi = (\psi_1, \psi_2, \psi_3)$ a 3-dimensional order parameter. Due to their definitions, states with $\psi_2 > 0$ and $\psi_3 \neq 3$ are impossible.

ψ_1	$\psi_2 = 0, \psi_3 =$				$\psi_3 = 3, \psi_2 =$															
	0	1	2	3	1	2	3	4	5	6	7	8	9	10	11	12	13	14	15	16
0	0	0	0	0	0	0	0	0	0	0	0	0	0	0	0	0	0	0	0	0
1	0	0	0	0	0	0	0	0	0	0	0	0	0	0	0	0	0	0	0	0
2	0	0	0	0	0	0	0	0	0	0	0	0	0	0	0	0	0	0	0	0
3	0	0	0	0	0	0	0	0	0	0	0	0	0	0	0	0	0	0	0	0
4	0	0	0	0	0	0	0	0	0	0	0	0	0	0	0	0	0	0	0	0
5	0	0	0	0	0	0	0	0	0	0	0	0	0	0	0	0	0	0	0	0
6	0	0	0	0	0	0	0	0	0	0	0	0	0	0	0	0	0	0	0	0
7	0	0	0	0	0	0	0	0	0	0	0	0	0	0	0	0	0	0	0	0
8	0	0	0	0	0	0	0	0	0	0	0	0	0	0	0	0	0	0	0	0
9	0	0	0	0	0	0	0	0	0	0	0	0	0	0	0	0	0	0	0	0
10	0	0	0	0	0	0	0	0	0	0	0	0	0	0	0	0	0	0	0	0
11	0	0	0	0	1	1	1	1	1	1	1	1	1	1	1	1	1	1	1	1
12	0	0	0	0	1	1	1	1	1	1	1	1	1	1	1	1	1	1	1	1
13	0	0	0	0	100	100	100	100	100	100	100	100	100	100	100	100	100	100	100	100
14	0	0	0	0	100	100	100	100	100	100	100	100	100	100	100	100	100	100	100	100
15	0	0	0	0	100	100	100	100	100	100	100	100	100	100	100	100	100	100	100	100
16	0	0	0	0	100	100	100	100	100	100	100	100	100	100	100	100	100	100	100	100
17	0	0	0	0	100	100	100	100	100	100	100	100	100	100	100	100	100	100	100	100
18	0	0	0	0	100	100	100	100	100	100	100	100	100	100	100	100	100	100	100	100
19	0	0	0	0	100	100	100	100	100	100	100	100	100	100	100	100	100	100	100	100
20	0	0	0	0	100	100	100	100	100	100	100	100	100	100	100	100	100	100	100	100

TABLE S8. Biasing potential $W(\psi)$ for window 2 of an overstepped walker without tension, with $\psi = (\psi_1, \psi_2, \psi_3)$ a 3-dimensional order parameter. Due to their definitions, states with $\psi_2 > 0$ and $\psi_3 \neq 3$ are impossible.

ψ_1	$\psi_2 = 0, \psi_3 =$				$\psi_3 = 3, \psi_2 =$															
	0	1	2	3	1	2	3	4	5	6	7	8	9	10	11	12	13	14	15	16
0	0	0	0	0	0	0	0	0	0	0	0	0	0	0	0	0	0	0	0	0
1	0	0	0	0	1	1	1	1	1	1	1	1	1	1	1	1	1	1	1	1
2	0	0	0	0	1	1	1	1	1	1	1	1	1	1	1	1	1	1	1	1
3	0	0	0	0	1	1	1	1	1	1	1	1	1	1	1	1	1	1	1	1
4	0	0	0	0	1	1	1	1	1	1	1	1	1	1	1	1	1	1	1	1
5	0	0	0	0	1	1	1	1	1	1	1	1	1	1	1	1	1	1	1	1
6	0	0	0	0	1	1	1	1	1	1	1	1	1	1	1	1	1	1	1	1
7	0	0	0	0	2	2	2	2	2	2	2	2	2	2	2	2	2	2	2	2
8	0	0	0	0	400	400	400	400	400	400	400	400	400	400	400	400	400	400	400	400
9	0	0	0	0	400	400	400	400	400	400	400	400	400	400	400	400	400	400	400	400
10	0	0	0	0	400	400	400	400	400	400	400	400	400	400	400	400	400	400	400	400
11	0	0	0	0	400	400	400	400	400	400	400	400	400	400	400	400	400	400	400	400
12	0	0	0	0	400	400	400	400	400	400	400	400	400	400	400	400	400	400	400	400
13	0	0	0	0	0	0	0	0	0	0	0	0	0	0	0	0	0	0	0	0
14	0	0	0	0	0	0	0	0	0	0	0	0	0	0	0	0	0	0	0	0
15	0	0	0	0	0	0	0	0	0	0	0	0	0	0	0	0	0	0	0	0
16	0	0	0	0	0	0	0	0	0	0	0	0	0	0	0	0	0	0	0	0
17	0	0	0	0	0	0	0	0	0	0	0	0	0	0	0	0	0	0	0	0
18	0	0	0	0	0	0	0	0	0	0	0	0	0	0	0	0	0	0	0	0
19	0	0	0	0	0	0	0	0	0	0	0	0	0	0	0	0	0	0	0	0
20	0	0	0	0	0	0	0	0	0	0	0	0	0	0	0	0	0	0	0	0

TABLE S9. Biasing potential $W(\psi)$ for window 3 of an overstepped walker without tension, with $\psi = (\psi_1, \psi_2, \psi_3)$ a 3-dimensional order parameter. Due to their definitions, states with $\psi_2 > 0$ and $\psi_3 \neq 3$ are impossible.

ψ_1	$\psi_2 = 0, \psi_3 =$				$\psi_3 = 3, \psi_2 =$															
	0	1	2	3	1	2	3	4	5	6	7	8	9	10	11	12	13	14	15	16
0	0	0	0	0	0	0	0	0	0	0	0	0	0	0	0	0	0	0	0	0
1	1	10	100	250	2.5×10^6	1×10^6	5×10^5	0	0	0	0	0	0	0	0	0	0	0	0	0
2	1	10	100	250	2.5×10^6	1×10^6	5×10^5	0	0	0	0	0	0	0	0	0	0	0	0	0
3	1	10	100	250	2.5×10^6	1×10^6	5×10^5	0	0	0	0	0	0	0	0	0	0	0	0	0
4	1	10	100	250	2.5×10^6	1×10^6	5×10^5	0	0	0	0	0	0	0	0	0	0	0	0	0
5	1	10	100	250	2.5×10^6	1×10^6	5×10^5	0	0	0	0	0	0	0	0	0	0	0	0	0
6	1	10	100	250	2.5×10^6	1×10^6	5×10^5	0	0	0	0	0	0	0	0	0	0	0	0	0
7	1	10	100	250	2.5×10^6	1×10^6	5×10^5	0	0	0	0	0	0	0	0	0	0	0	0	0
8	1	10	100	250	2.5×10^6	1×10^6	5×10^5	0	0	0	0	0	0	0	0	0	0	0	0	0
9	1	10	100	250	2.5×10^6	1×10^6	5×10^5	0	0	0	0	0	0	0	0	0	0	0	0	0
10	1	10	100	250	2.5×10^6	1×10^6	5×10^5	0	0	0	0	0	0	0	0	0	0	0	0	0
11	1	10	100	250	2.5×10^6	1×10^6	5×10^5	0	0	0	0	0	0	0	0	0	0	0	0	0
12	1	10	100	250	2.5×10^6	1×10^6	5×10^5	0	0	0	0	0	0	0	0	0	0	0	0	0
13	1	10	100	250	2.5×10^6	1×10^6	5×10^5	0	0	0	0	0	0	0	0	0	0	0	0	0
14	1	10	100	250	2.5×10^6	1×10^6	5×10^5	0	0	0	0	0	0	0	0	0	0	0	0	0
15	1	10	100	250	2.5×10^6	1×10^6	5×10^5	0	0	0	0	0	0	0	0	0	0	0	0	0
16	1	10	100	250	2.5×10^6	1×10^6	5×10^5	0	0	0	0	0	0	0	0	0	0	0	0	0
17	1	10	100	250	2.5×10^6	1×10^6	5×10^5	0	0	0	0	0	0	0	0	0	0	0	0	0
18	1	10	100	250	2.5×10^6	1×10^6	5×10^5	0	0	0	0	0	0	0	0	0	0	0	0	0
19	1	10	100	250	2.5×10^6	1×10^6	5×10^5	0	0	0	0	0	0	0	0	0	0	0	0	0
20	1	10	100	250	2.5×10^6	1×10^6	5×10^5	0	0	0	0	0	0	0	0	0	0	0	0	0

TABLE S10. Biasing potential $W(\psi)$ for window 1 of an overstepped walker with tension, with $\psi = (\psi_1, \psi_2, \psi_3)$ a 3-dimensional order parameter. Due to their definitions, states with $\psi_2 > 0$ and $\psi_3 \neq 3$ are impossible.

ψ_1	$\psi_2 = 0, \psi_3 =$				$\psi_3 = 3, \psi_2 =$															
	0	1	2	3	1	2	3	4	5	6	7	8	9	10	11	12	13	14	15	16
0	0	0	0	0	0	0	0	0	0	0	0	0	0	0	0	0	0	0	0	0
1	0	0	0	0	0	0	0	0	0	0	0	0	0	0	0	0	0	0	0	0
2	0	0	0	0	0	0	0	0	0	0	0	0	0	0	0	0	0	0	0	0
3	0	0	0	0	0	0	0	0	0	0	0	0	0	0	0	0	0	0	0	0
4	0	0	0	0	0	0	0	0	0	0	0	0	0	0	0	0	0	0	0	0
5	0	0	0	0	0	0	0	0	0	0	0	0	0	0	0	0	0	0	0	0
6	0	0	0	0	0	0	0	0	0	0	0	0	0	0	0	0	0	0	0	0
7	0	0	0	0	0	0	0	0	0	0	0	0	0	0	0	0	0	0	0	0
8	0	0	0	0	0	0	0	0	0	0	0	0	0	0	0	0	0	0	0	0
9	0	0	0	0	0	0	0	0	0	0	0	0	0	0	0	0	0	0	0	0
10	0	0	0	0	0	0	0	0	0	0	0	0	0	0	0	0	0	0	0	0
11	0	0	0	0	3	3	3	3	3	3	3	3	3	3	3	3	3	3	3	3
12	0	0	0	0	3	3	3	3	3	3	3	3	3	3	3	3	3	3	3	3
13	0	0	0	0	250	250	250	250	250	250	250	250	250	250	250	250	250	250	250	250
14	0	0	0	0	400	400	400	400	400	400	400	400	400	400	400	400	400	400	400	400
15	0	0	0	0	600	600	600	600	600	600	600	600	600	600	600	600	600	600	600	600
16	0	0	0	0	1000	1000	1000	1000	1000	1000	1000	1000	1000	1000	1000	1000	1000	1000	1000	1000
17	0	0	0	0	2000	2000	2000	2000	2000	2000	2000	2000	2000	2000	2000	2000	2000	2000	2000	2000
18	0	0	0	0	4000	4000	4000	4000	4000	4000	4000	4000	4000	4000	4000	4000	4000	4000	4000	4000
19	0	0	0	0	20000	20000	20000	20000	20000	20000	20000	20000	20000	20000	20000	20000	20000	20000	20000	20000
20	0	0	0	0	20000	20000	20000	20000	20000	20000	20000	20000	20000	20000	20000	20000	20000	20000	20000	20000

TABLE S11. Biasing potential $W(\psi)$ for window 2 of an overstepped walker with tension, with $\psi = (\psi_1, \psi_2, \psi_3)$ a 3-dimensional order parameter. Due to their definitions, states with $\psi_2 > 0$ and $\psi_3 \neq 3$ are impossible.

ψ_1	$\psi_2 = 0, \psi_3 =$				$\psi_3 = 3, \psi_2 =$															
	0	1	2	3	1	2	3	4	5	6	7	8	9	10	11	12	13	14	15	16
0	0	0	0	0	0	0	0	0	0	0	0	0	0	0	0	0	0	0	0	0
1	0	0	0	0	1	1	1	1	1	1	1	1	1	1	1	1	1	1	1	1
2	0	0	0	0	1	1	1	1	1	1	1	1	1	1	1	1	1	1	1	1
3	0	0	0	0	1	1	1	1	1	1	1	1	1	1	1	1	1	1	1	1
4	0	0	0	0	1	1	1	1	1	1	1	1	1	1	1	1	1	1	1	1
5	0	0	0	0	1	1	1	1	1	1	1	1	1	1	1	1	1	1	1	1
6	0	0	0	0	1	1	1	1	1	1	1	1	1	1	1	1	1	1	1	1
7	0	0	0	0	2	2	2	2	2	2	2	2	2	2	2	2	2	2	2	2
8	0	0	0	0	400	400	400	400	400	400	400	400	400	400	400	400	400	400	400	400
9	0	0	0	0	300	300	300	300	300	300	300	300	300	300	300	300	300	300	300	300
10	0	0	0	0	300	300	300	300	300	300	300	300	300	300	300	300	300	300	300	300
11	0	0	0	0	300	300	300	300	300	300	300	300	300	300	300	300	300	300	300	300
12	0	0	0	0	300	300	300	300	300	300	300	300	300	300	300	300	300	300	300	300
13	0	0	0	0	0	0	0	0	0	0	0	0	0	0	0	0	0	0	0	0
14	0	0	0	0	0	0	0	0	0	0	0	0	0	0	0	0	0	0	0	0
15	0	0	0	0	0	0	0	0	0	0	0	0	0	0	0	0	0	0	0	0
16	0	0	0	0	0	0	0	0	0	0	0	0	0	0	0	0	0	0	0	0
17	0	0	0	0	0	0	0	0	0	0	0	0	0	0	0	0	0	0	0	0
18	0	0	0	0	0	0	0	0	0	0	0	0	0	0	0	0	0	0	0	0
19	0	0	0	0	0	0	0	0	0	0	0	0	0	0	0	0	0	0	0	0
20	0	0	0	0	0	0	0	0	0	0	0	0	0	0	0	0	0	0	0	0

TABLE S12. Biasing potential $W(\psi)$ for window 3 of an overstepped walker with tension, with $\psi = (\psi_1, \psi_2, \psi_3)$ a 3-dimensional order parameter. Due to their definitions, states with $\psi_2 > 0$ and $\psi_3 \neq 3$ are impossible.

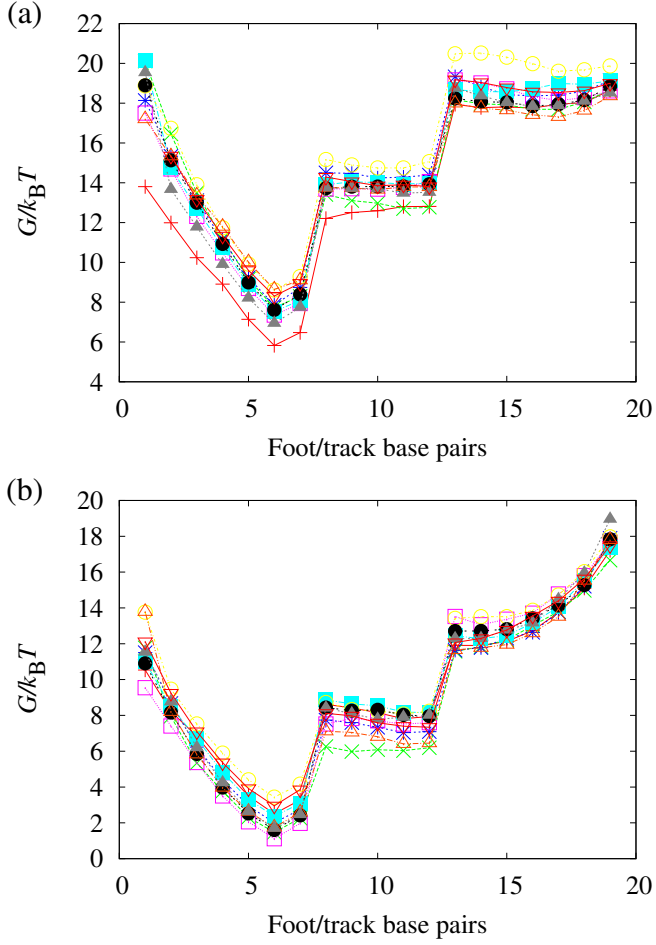


FIG. S13. Results of 10 independent estimates of the free-energy profile (G) for fuel displacement of the track; (a) without tension and (b) with the track under 14.6 pN of tension. The combination of the ten separate estimates into a single profile for each case is shown in Fig. 10 of the main text. Free energies are given as a function of the number of foot/track base pairs (ψ_1), subject to the constraint that the fuel is bound to the foot by at least one base pair ($\psi_2 > 0$, $\psi_3 = 3$). Free energies are reported relative a system without bound fuel ($\psi_2 = 0$, $\psi_3 = 0, 1, 2, 3$).